

7 Unraveling a Biomass-Derived Multiphase Catalyst
8
11 for the Dehydrogenative Coupling of Silanes with
12
13
14
15 Alcohols under Aerobic Conditions
16
17
18

19 *Iván Sorribes,^{*,a,†} David Ventura-Espinosa,^b Marcelo Assis,^c Santiago Martín,^{d,e} Patricia*
20
21

22 *Concepción,^f Jefferson Bettini,^g Elson Longo,^c Jose A. Mata,^b Juan Andrés^a*
23
24
25

26
27 ^aDepartament de Química Física i Analítica, Universitat Jaume I, Av. Sos Baynat s/n,
28
29
30
31 12071, Castellón, Spain
32
33

34 ^bInstitute of Advanced Materials (INAM), Universitat Jaume I, Av. Sos Baynat s/n, 12071,
35
36
37 Castellón, Spain
38
39
40

41 ^cCenter for Development of Functional Materials (CDMF), Federal University of São
42
43
44 Carlos, P.O. Box 676, 13565-905, São Carlos, SP, Brazil
45
46
47

48 ^dInstituto de Nanociencia y Materiales de Aragón (INMA), CSIC-Universidad de
49
50
51 Zaragoza, 50009, Zaragoza, Spain
52
53
54

55 ^eDepartamento de Química Física, Universidad de Zaragoza, 50009, Zaragoza, Spain
56
57
58
59
60

^fInstituto de Tecnología Química, Universitat Politècnica de València-Consejo Superior de Investigaciones Científicas, Av. De los Naranjos, s/n, 46022, Valencia, Spain

^gBrazilian Nanotechnology National Laboratory (LNNano), R. Guiuseppe Maximo Scolfaro 10000, 13083-970, Campinas, Brazil

[†]Present address: Instituto de Tecnología Química, Universitat Politècnica de València-Consejo Superior de Investigaciones Científicas, Av. De los Naranjos, s/n, 46022, Valencia, Spain

Corresponding Author

* Corresponding author. E-mail address: isorribe@uji.es; ivsorter@itq.upv.es

KEYWORDS: Chitosan, Silanes, Alcohols, Dehydrogenative coupling, Silyl ethers, Oxygen activation, *in-situ* Raman spectroscopy

ABSTRACT: Herein, a novel silver and chromium nanostructured N-doped carbonaceous material has been synthesized by a biomass-annealing approach using readily available chitosan as a raw material. The resulting catalyst AgCr@CN-800 has been applied for

the dehydrogenative coupling reaction of various silanes with different alcohols to obtain the corresponding silyl ethers under aerobic and mild conditions. Besides excellent activity and selectivity, the as-prepared catalyst exhibits good stability and reusability. Characterization by XRD, XPS, ICP-MS, HRTEM, in combination with careful examination of the structure with Cs-corrected HAADF-STEM revealed that catalyst AgCr@CN-800 comprises Ag and CrN aggregated particles, as well as highly dispersed Ag-N_x and Cr-N_x sites embedded in N-doped graphitic structures. A comparative catalytic study using structure-related catalysts in combination with acid-leaching treatments has shown that the most active species are the Ag particles, and that their activity is boosted by the presence of Cr-derived species. By *in-situ* Raman spectroscopy experiments, it has been found that the dehydrogenative coupling of silanes with alcohols in the presence of catalyst AgCr@CN-800 takes place through an oxygen-assisted mechanism.

INTRODUCTION

1
2
3
4 Silyl ethers are valuable raw materials for the silicon industry as well as important
5
6
7 commodity reagents and protecting groups for alcohols in organic synthesis on laboratory
8
9
10 scale.¹⁻⁵ In addition, these compounds have also attracted the attention of scientists from
11
12
13 the perspective of material science because of their use as reagents for surface coating
14
15
16 and modification,⁶⁻¹³ as well as for the preparation of hybrid organic–inorganic
17
18
19 materials.¹⁴⁻¹⁶
20
21
22
23

24 Traditionally, silyl ethers have been synthesized by reaction of halosilanes with alcohols
25
26
27 in the presence of a base, thus resulting in the formation of stoichiometric amounts of
28
29
30 undesired halide salts.¹⁷⁻²⁰ In this context, the catalytic dehydrogenative coupling of
31
32
33 hydrosilanes with alcohols represents a more atom-economical, and hence, a more
34
35
36 environmental-friendly synthetic route.²¹⁻²² Advantageously, since hydrogen is the only
37
38
39 generated by-product, this reaction is also relevant for H₂-generation. In fact, the system
40
41
42 based on alcohol/silane pairs has been considered as a potential liquid organic hydrogen
43
44
45 carrier (LOHCs) that releases H₂ at low temperatures.²³⁻²⁴ However, although this
46
47
48 coupling reaction is thermodynamically favored, the presence of a catalyst is required to
49
50
51 improve the reaction kinetics under mild conditions.
52
53
54
55
56
57
58
59
60

1
2
3
4 To date, a wide variety of transition-metal-based complexes,²⁵⁻³⁶ alkaline earth
5
6
7 metals,³⁷ and alkali metal bases³⁸⁻³⁹ have been reported as catalysts for the
8
9
10 dehydrogenative coupling of hydrosilanes with alcohols. Moreover, metal-free boron-
11
12
13 based Lewis acids⁴⁰⁻⁴³ and N-heterocyclic carbenes⁴⁴ have also efficiently catalyzed this
14
15
16 reaction. Nevertheless, despite good activity and selectivity toward the production of silyl
17
18
19 ethers achieved by these catalysts, the use of reusable heterogeneous systems is more
20
21
22 advantageous from an environmental point of view.
23
24
25
26

27
28 In recent times, with the aim of dealing with global challenges related to sustainability,
29
30
31 the scientific community has paid much attention toward the use of metal nanoparticles
32
33
34 (NPs) modified by N-doped carbon as catalysts for innovative organic synthesis because
35
36
37 of their good activity and controllable selectivity.⁴⁵ Different strategies have been
38
39
40 developed for the preparation of this kind of nanostructured materials.⁴⁶ Among them, the
41
42
43 *in-situ* formation of both metal NPs and the N-doped graphitic material is a well-
44
45
46 established methodology. Here, non-volatile molecularly defined metal-amine ligated
47
48
49 complexes impregnated on different supports,⁴⁷⁻⁸¹ metal-organic frameworks (MOFs),⁸²⁻
50
51
52
53
54
55
56
57
58
59
60

1
2
3
4 ⁹² or coordination polymers⁹³⁻⁹⁵ are typically used as self-sacrificial templates to obtain
5
6
7 metal NPs embedded in a carbonaceous matrix after pyrolysis under an inert gas.
8
9

10 Alternatively, in order to avoid the use of sophisticated organic ligands and synthetically
11
12
13
14 demanding routes of sacrificial template materials, pyrolysis of renewable and available
15
16
17 biomass in combination with metal salts represents a more practical catalyst preparation
18
19
20 approach.⁹⁶⁻¹⁰⁵ In this respect, the natural biopolymer chitosan, which is obtained from
21
22
23
24 industrial fishery bio-waste by deacetylation of shrimp or crab shell-derived chitin, is
25
26
27 especially useful.¹⁰⁶ Chitosan has been proposed as an attractive precursor for obtaining
28
29
30
31 N-doped carbon materials.¹⁰⁷⁻¹²² In addition, its particular structure containing amino- and
32
33
34
35 hydroxyl-coordinating groups has made possible its application as a chelating agent for
36
37
38 transition-metals.¹²³⁻¹²⁸
39
40
41

42 Taking advantage of these properties of chitosan, Garcia and co-workers synthesized
43
44
45 Cu NPs supported on N-doped graphene by firstly preparing a homogeneous solution of
46
47
48
49 a Cu salt and chitosan, followed by pyrolysis and sonication.¹²⁹ Later, the same group
50
51
52 developed a series of facet-oriented Cu₂O,¹³⁰⁻¹³² Au,¹³³ Pt,¹³⁴ and Ag¹³⁵ NPs on (N-doped)
53
54
55
56 graphene films prepared by pyrolysis of nanometer-thick films of chitosan embedding the
57
58
59
60

corresponding transition-metal salt and deposited on a quartz substrate. Importantly, a variation or even a completely removal of the N content was reported depending on the pyrolysis temperature and the metal nature. Meanwhile, Beller and co-workers prepared Co-based N-doped carbon heterogeneous catalysts by using an adapted synthetic methodology, in which chitosan acts as a solid adsorbent for transition metals instead of being used in solution before pyrolysis.¹³⁶⁻¹³⁹ In addition to these seminal works, other catalytic materials synthesized following a similar preparation approach have also been reported.¹⁴⁰⁻¹⁴⁹

In general, metal-based materials prepared by pyrolysis tend to be heterogeneous in composition and particle size. In fact, the resulting materials are typically constituted by metal species of different nature, such as metallic and/or metal oxide NPs. Moreover, the formation of isolated single-atom sites (ISAS) is also feasible when using supports or self-sacrificial templates that have a strong coordination ability with metal atoms.¹⁵⁰⁻¹⁵⁸ Concretely, this is the case of chitosan, in which its unique structure containing amino- and hydroxyl-coordinating groups can promote the formation of ISAS embedded in the N-doped carbon matrix besides other multiple metal species formed by agglomeration

1
2
3 during uncontrolled pyrolysis.¹⁵⁹⁻¹⁶⁰ This heterogeneity in chitosan-derived N-doped
4
5
6
7 carbon-based materials makes challenging the identification of active species when they
8
9
10 are used in catalysis, however, it is an essential task for future development of catalysts
11
12
13
14 with enhanced efficiency.
15

16
17 With regard to the use of heterogeneous catalysts for the dehydrogenative coupling
18
19
20 reaction of hydrosilanes with alcohols, among various available heterogeneous
21
22
23 systems,^{36, 161-179} metal catalysts modified by (doped) graphitic carbon have shown
24
25
26 promising results. Cu NPs supported on doped (-boron and/or -nitrogen) graphene,¹²⁹
27
28
29
30
31 Cu₂O¹³⁰ or Ag¹³⁵ facet-oriented nanoplatelets on graphene films, as well as, atomically
32
33
34 dispersed Co species anchored on ultrathin two-dimensional N-doped carbon¹⁸⁰ have
35
36
37 been proved to be active catalysts for the title reaction. In addition, the use of a metal-
38
39
40
41 free hierarchically porous N and S co-doped carbon is also noteworthy.¹⁸¹ Despite these
42
43
44 findings, the relatively high temperature, long reaction times, the need to perform the
45
46
47 reaction under inert atmosphere, and/or the difficulty of preparing catalysts with higher
48
49
50
51 metal loading offer room for improvement.
52
53
54
55
56
57
58
59
60

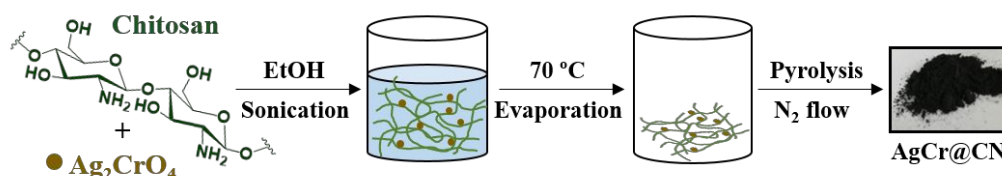
1
2
3 In this contribution, we report the preparation of a N-doped carbonaceous
4
5
6
7 heterobimetallic nanostructured material by pyrolysis of silver chromate (Ag_2CrO_4) highly
8
9
10 dispersed on the readily available bio-waste polymer chitosan. We show that the resulting
11
12
13 material, which comprises a heterogeneous composition of metal species, efficiently
14
15
16
17 catalyzes the dehydrogenative coupling of hydrosilanes with alcohols under aerobic and
18
19
20 mild conditions (even at 0 °C) with excellent selectivity toward the formation of silyl ethers
21
22
23 and molecular hydrogen. On the bases of a comparative catalytic study, we demonstrate
24
25
26
27 that catalytic activity mainly arises from the Ag particles and that their activity is boosted by
28
29
30 the presence of Cr-derived species. Furthermore, *in-situ* Raman spectroscopic studies have allowed
31
32
33 the explanation of the enhanced catalytic activity, which is directly related with the oxygen
34
35
36 activation ability of the catalyst.
37
38

39 RESULTS AND DISCUSSION 40 41

42 Preparation and catalytic performance of catalysts AgCr@CN 43 44

45 We started our study by preparing a series of silver and chromium bimetallic catalysts
46
47
48 according to the procedure depicted in Scheme 1. A mixture of chitosan and Ag_2CrO_4
49
50
51 was homogeneously dispersed in ethanol by sonication. After solvent evaporation under
52
53
54
55
56
57
58
59
60

atmospheric pressure and continuous stirring conditions, the resultant powder was pyrolyzed at different temperatures in the range from 400 to 900 °C under a nitrogen flow to yield the heterobimetallic materials AgCr@CN-X, where X stands for the pyrolysis temperature (see the Experimental Section for more preparation details). The metal content in the as-prepared materials was determined by inductively coupled plasma mass spectrometry (ICP-MS) analysis. The obtained results revealed an increase of the metal amount (Ag + Cr) from 13.7 to 18.0 wt% with the pyrolysis temperature because of increasing weight loss in chitosan decomposition (Table S1). Interestingly, the Ag/Cr ratio is maintained constant independently of the pyrolysis temperature.



Scheme 1. Synthesis of heterobimetallic materials AgCr@CN-X (X = 400-900 °C) used as catalysts.

With these materials in hand, we evaluated their catalytic performance for the dehydrogenative coupling of hydrosilanes with alcohols using as a benchmark system the reaction between dimethyl(phenyl)silane (**1a**) and methanol (**2a**) at 60 °C under aerobic conditions. As shown in

Figure 1a, all prepared heterobimetallic materials displayed catalytic activity with excellent selectivity toward the formation of methoxydimethyl(phenyl)silane (**3aa**) (see also Figure S1). A control experiment revealed that no reaction took place in the presence of a metal-free catalyst (M-free@CN-800) prepared by pyrolysis of chitosan at 800 °C in the absence of Ag₂CrO₄, thus indicating that the catalytically active species are metal-based. The most active catalyst, determined by comparison of the initial reaction rates normalized to the mass of metal weights (Figure 1b), resulted to be the heterobimetallic material pyrolyzed at 800 °C (AgCr@CN-800). Other heterobimetallic catalysts containing silver and a second transition metal different to chromium (W or V), which were also prepared following the same preparation methodology shown in Scheme 1, displayed lower activity for the investigated reaction (Figure S2).

In the presence of the most active catalyst AgCr@CN-800 (15 mg; 2.75 mol% of metal with respect to **1a**), full conversion of **1a** was achieved in 20 min, affording **3aa** in 97 % yield with only residual amounts (< 3 %) and traces (< 1 %) of the corresponding silanol (**4a**) and disiloxane (**5a**) compounds as by-products, respectively (Figure 1c). Moreover, H₂ release was also detected during the reaction between **1a** and **2a**. This dehydrogenative coupling reaction also proceeds well when using lower amounts of catalyst AgCr@CN-800 (5 mg; 0.91 mol% of metal with respect to **1a**), corresponding to a turnover number (TON) of 111. Interestingly, the reaction could also be conducted at lower temperature, 30 °C and even 0 °C, achieving full conversion of **1a** with excellent selectivity to **3aa** in 1 and 2 h, respectively (Figure S3), together with the formation of equimolecular amounts of H₂ (see the Supporting Information). It is worth mentioning that compared to previously reported Ag-based heterogeneous systems, the catalyst AgCr@CN-800 catalyzes this reaction at significant lower temperatures (0 °C).^{135, 172, 182-185}

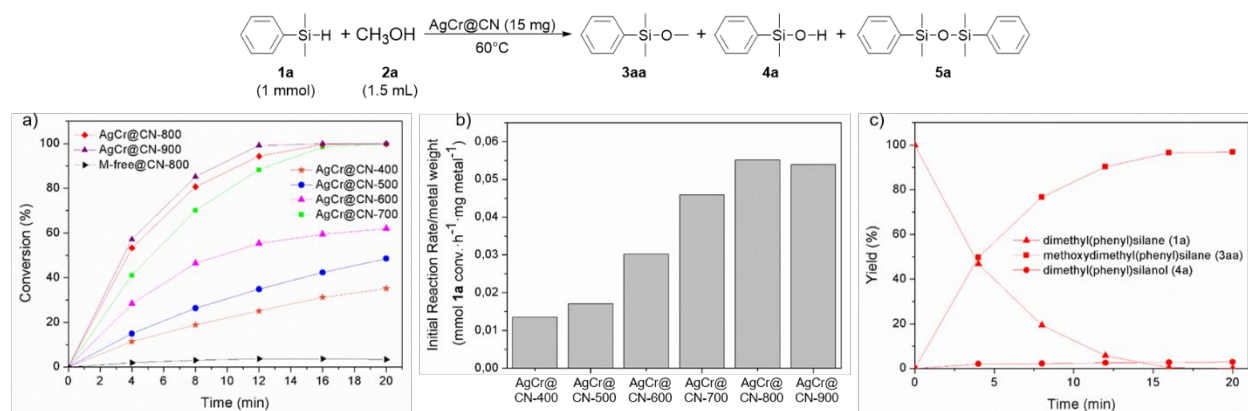


Figure 1. (a) Catalytic performances of catalysts AgCr@CN-X (X = 400-900) and M-free@CN-800 for the dehydrogenative coupling reaction of **1a** with methanol. (b) Comparison of the metal mass activity. (c) Concentration/time diagram for catalyst AgCr@CN-800.

Interestingly, the reaction rate was significantly increased when pure O₂ was bubbled into the reaction solution providing a 98 % yield of **3aa** within 20 min at 30 °C (TOF = 327 h⁻¹). In contrast, almost no reaction took place when the reaction was carried out under Ar atmosphere, thus revealing that the presence of the catalyst AgCr@CN-800 in combination with O₂ is essential to achieve the dehydrogenative coupling reaction of **1a** with methanol (Figure S3).

Characterization of catalyst AgCr@CN-800

The best heterobimetallic material AgCr@CN-800 in terms of catalytic activity was characterized in detail. The XRD pattern (Figure 2) is dominated by the presence of diffraction peaks associated with the face-centered cubic (*fcc*) structure of Ag⁰ in agreement with the JCPDS database (PDF Card 1-1164). Since these peaks are very sharp, it is expected that this phase is present in the form of large particles. Moreover, a broad shoulder peak in the range of 20–30° (2θ) associated with reflections of the (002) of graphitic carbon could also be inferred.¹⁸⁶ However, no additional peaks corresponding to chromium species were detected.

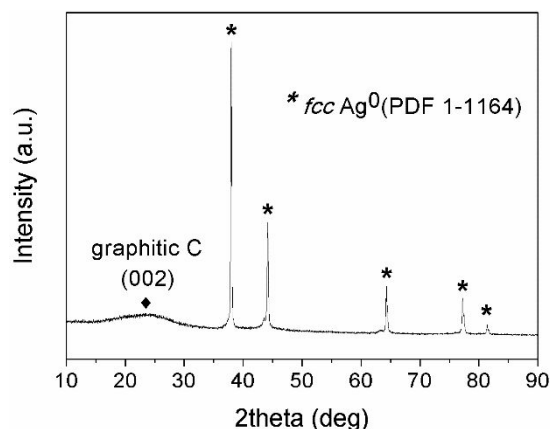


Figure 2. XRD pattern for catalyst AgCr@CN-800.

Transmission electron microscopy (TEM) images show aggregates of metal particles with non-homogeneous sizes of tens to hundreds of nanometers. This broad size distribution is likely generated by partial metal agglomeration during the pyrolysis treatment because of the high metal content (Figures 3a and Figure S4). The high-resolution TEM (HRTEM) images show two types of metal particles of different nature, both coated by few layers of a (defect/N-doped) graphitic carbon shell (Figure 3b-c). The well-resolved lattice spacing of 0.237 nm consistent with the (111) plane of the cubic Ag phase was clearly identified in some of these particles. Besides, an additional phase of chromium nitride (CrN) that displays the characteristic lattice spacing of 0.239 nm associated with its (111) plane was also detected in the HRTEM images. Moreover, the nature of these particles was undoubtedly confirmed by a fast Fourier transform (FFT) analysis, which revealed other characteristic lattice fringe spaces of 0.211 and 0.128 nm associated with the (200) and (311) planes of CrN, respectively (Figure 3c, inset).

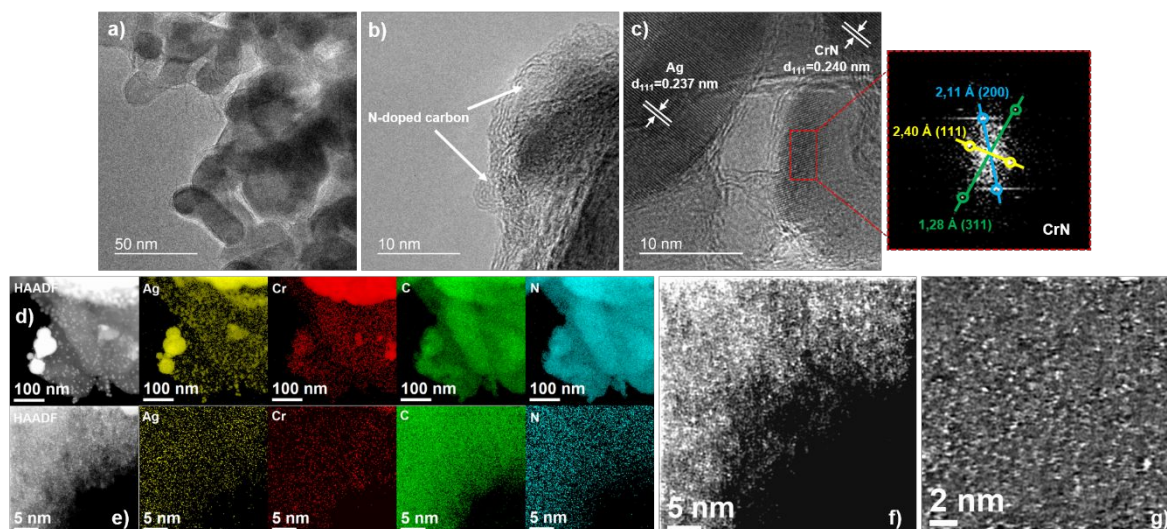


Figure 3. Electron microscopy characterization of catalyst AgCr@CN-800. TEM (a) and HRTEM (b-c) micrographs. The inset shows the FFT from the square region in image c). (d-e) HAADF-STEM images and EDS elemental mapping of Ag, Cr, C, and N. (f-g) High-magnification images for the Cs-corrected HAADF-STEM analysis.

Spherical aberration (Cs)-corrected scanning transmission electron microscopy (STEM) using a high-angle annular dark-field (HAADF) detector coupled with spectroscopic analysis by means of energy dispersive X-ray spectroscopy (EDS) was employed to investigate the structure of catalyst AgCr@CN-800 in a further extent. These studies revealed that Ag, Cr, N, and C elements overlap in spatial locations on each other around the entire sample, including particles (Figure 3d and Figure S5) as well as sites where no particles were visualized (Figure 3e and Figure S5), thus suggesting that metal species may be atomically distributed along the N-doped graphitic material. Interestingly, a closer look at these regions revealed a high density of monodispersed bright dots, likely associated with highly dispersed metal atoms of both Ag and Cr, according to the EDS elemental mapping analysis results (Figure 3f-g and Figure S6-S7).

For further characterization of the catalyst surface, X-ray photoelectron spectroscopy (XPS) measurements were performed. The high-resolution Ag 3d core level spectrum displays two peaks at \square 368 and 374 eV associated with the characteristic spin–orbit splitting of Ag 3d_{5/2} and Ag 3d_{3/2} orbitals, respectively, each of them being possible to be fitted into two separated components denoting the presence of two distinct chemical Ag species (Figure 4a). More specifically, the components at 368.1 and 374.1 eV correspond to Ag⁺ species, whereas the ones at 369.3 and 375.3 eV are related to metallic Ag.¹⁸⁷⁻¹⁹¹ The higher contribution of the component associated with Ag⁺ species suggests that, in spite of the shielding effect of thick N-doped graphitic carbon layers encapsulating the Ag particles, these could be constituted by a metallic core and a partially oxidized surface. In addition, it should be considered that the XPS-detectable Ag⁺ species could also arise from highly dispersed Ag⁺ species inserted in the graphitic sheets coordinated to N atoms, that is, as AgN_x sites. Comparison of the obtained electron binding energy of Ag 3d_{5/2} (368.1 eV) in catalyst AgCr@CN-800 with that one for previously reported molecular-defined complexes that contain Ag-N bonds within a related structure (368.4 eV),¹⁹² revealed a prominent increase of the electron density of the Ag⁺ species in the graphitized structure, in good agreement with previous studies.¹⁵⁰

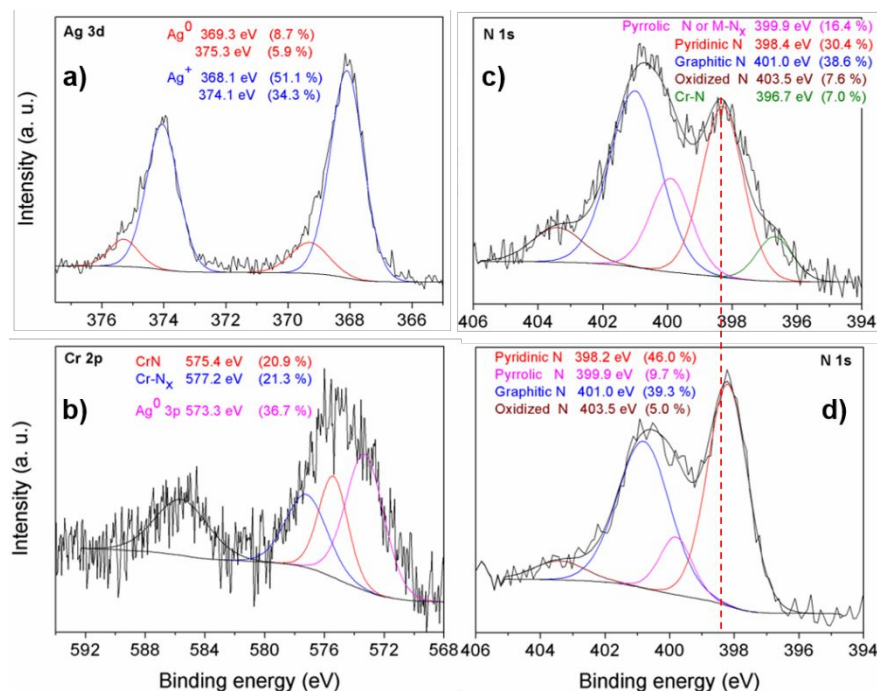


Figure 4. XPS spectra of Ag 3d (a), Cr 2p (b) and N 1s (c) core levels of catalyst AgCr@CN-800. (d) N 1s XPS spectrum of catalyst M-free@CN-800.

Determination of Cr oxidation states in heterobimetallic materials containing Ag is challenging because in the Cr 2p region of the XPS spectrum some Cr species have similar electron binding energy values than that of the Ag 3p peak (573.6 eV) associated with metallic Ag. The Cr 2p XPS spectrum (Figure 4b) for catalyst AgCr@CN-800 shows a broad peak, which could be fitted into three different components after deconvolution. The major peak at 573.3 eV can be ascribed to metallic Ag, whereas, according to the literature, the other two peaks at 575.4 and 577.2 eV denote the presence of CrN¹⁹³ and atomically dispersed Cr-N_x sites embedded in the graphitic sheets,¹⁹⁴ respectively.

The signal deconvolution in the high-resolution N 1s energy-level spectrum (Figure 4c) suggests that catalyst AgCr@CN-800 contains different nitrogen species, at least including pyridinic N-oxide (403.5 eV), graphitic-N (401.0 eV), pyrrolic-N (399.9 eV) and pyridinic-N (398.4 eV).

Furthermore, an additional component (at 396.7 eV) attributed to CrN could also be inferred, which is absent in the XPS spectrum of the metal-free catalyst M-free@CN-800 (Figure 4d). Importantly, further comparison of both spectra (Figure 4c and 4d) revealed that while the relative content of graphitic-N and pyridinic N-oxide species is almost the same, an increase of the ratio of pyrrolic-N to pyridinic-N species is observed in catalyst AgCr@CN-800. This increase could be associated with the presence of highly dispersed species attached to pyridinic-N that results in the formation of M-N_x (M = Ag, Cr) sites, whose binding energies fall in the same range as the pyrrolic-N function binding energy. Moreover, an energy shift of over 0.2 eV was detected in the pyridinic-N component of catalyst AgCr@CN-800, thus verifying the existence of metal-N interactions.^{150,152,195}

Acid-leaching and characterization of catalyst AgCr@CN-800-Acid

Catalyst AgCr@CN-800 was leached with acid (see details in the Experimental Section) and further characterized. The Ag and Cr content, determined by ICP-MS analysis, in the leached catalyst (denoted as AgCr@CN-800-Acid) were reduced from 12.74 to 0.12 wt% and from 3.74 to 2.29 wt%, respectively. In consequence, no diffraction peaks associated with metallic Ag species were detected in the XRD pattern of the acid-leached catalyst AgCr@CN-800-Acid (Figure 5a). However, besides the broad diffraction peaks of graphitic carbon (at 2 θ values of 25.3 and 43.6°), other peaks located at 37.5, 43.6, 63.4 and 76.1°, that could be indexed to the (111), (200), (220) and (311) planes, respectively, of the cubic phase of CrN (PDF Card 65-2899), became known in catalyst AgCr@CN-800-acid. This confirms that the acid-leaching treatment fully removed the Ag particles, while keeping almost intact the CrN phase, which is known to display an excellent chemical stability to acids.¹⁹⁶⁻¹⁹⁷

The diffraction peaks associated with CrN are also present in the XRD pattern measured after the acid treatment of a catalyst (AgCr@CN-800-Ar) pyrolyzed under Ar atmosphere instead of using N₂ (see Figure S8). This result, besides the fact that only a slight decrease of the N content (determined by combustion elemental analysis) was detected in catalyst AgCr@CN-800-Ar (7.6 wt %) when comparing with catalyst AgCr@CN-800 (7.8 wt %), proves that the CrN phase is preferentially formed during the pyrolysis treatment by extracting N atoms from chitosan rather than by activation of N₂ gas molecules. Moreover, both catalysts AgCr@CN-800 and AgCr@CN-800-Ar displayed similar catalytic performance for the investigated dehydrogenative coupling reaction between dimethylphenylsilane (**1a**) and methanol (see Figure S8).

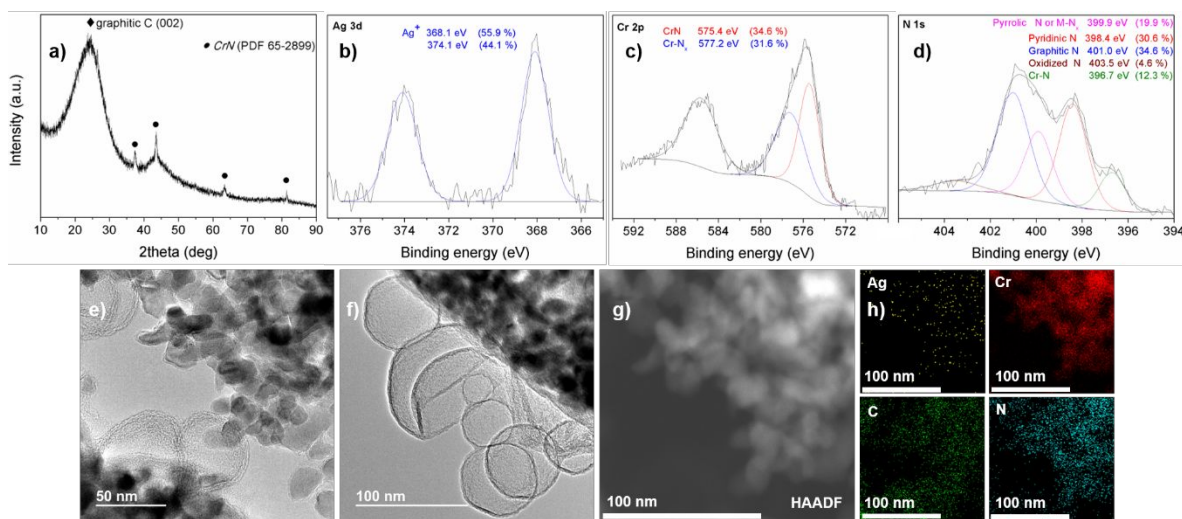


Figure 5. Characterization of catalyst AgCr@CN-800-Acid. (a) XRD spectrum. Ag 3d (b), Cr 2p (c) and N 1s (d) core level XPS spectra. TEM (e, f) and HAADF-STEM (g) images. (h) EDS elemental mapping of Ag, Cr, C, and N.

Morphological characterization of the acid-etched catalyst AgCr@CN-800-Acid by TEM showed the presence of coated nanoparticles (30 nm) as well as hollow-centered (defect/N-doped) graphitic carbon layers (Figure 5e-f). These empty carbonaceous spheres result from the

leaching of Ag particles, further confirming the core-shell structure of this heterobimetallic material. The elemental distribution of catalyst AgCr@CN-800-Acid was investigated by EDS elemental mapping (Figure 5g-h), and confirms that, as in the case of catalyst AgCr@CN-800, Cr, C and N elements overlap well in spatial locations, while monodispersed Ag is present in a considerably lower amount, in good agreement with the ICP-MS analysis.

Interestingly, the Ag 3d core level XPS spectrum of catalyst AgCr@CN-800-acid discloses the only presence of Ag⁺ ionic species (i.e. AgN_x sites) represented as two peaks with electron-binding energy values of 368.1 and 374.1 eV after deconvolution and fitting (Figure 5b). It should be noted that the component associated with the Ag 3p peak (573.6 eV) of metallic Ag completely disappeared from the Cr 2p core level XPS spectrum (Figure 5c), being possible to fit the observed peak into two only components corresponding to CrN (575.4 eV) and to atomically dispersed Cr-N_x sites embedded in the graphitic carbon (577.2 eV). On the contrary, no relevant changes are observed in the high-resolution N 1s energy-level spectrum after the acid leaching treatment (Figure 5d).

Based on all characterization results before and after the acid-leaching treatment, we can conclude that catalyst AgCr@CN-800 is a heterobimetallic N-doped carbonaceous material, in which different metal species coexist. More specifically, catalyst AgCr@CN-800 comprises Ag and CrN aggregated particles covered by few layers of defect N-doped graphitic carbon containing highly dispersed Ag-N_x and Cr-N_x species as well.

Probing into the metal active species

To unveil which of these species is catalytically active for the investigated dehydrogenative coupling reaction between dimethylphenylsilane (**1a**) and methanol (**2a**) to afford methoxydimethyl(phenyl)silane (**3aa**), the titled reaction was carried out in the presence of

different catalysts (see the Experimental Section and the Supporting Information for preparation and characterization details, respectively). As shown in Figure 6a, a significant decrease of the initial reaction rate (normalized to the mass of metal weights) was achieved by using the acid-etched catalyst AgCr@CN-800-Acid. Nevertheless, it is worth mentioning that reaction proceeded with excellent selectivity after longer reaction times (Figure 6b). Since Ag particles are the species removed with the acid-leaching treatment, this result denotes that they are required for the high activity of catalyst AgCr@CN-800, while the remaining species (i.e. CrN particles and highly dispersed CrN_x and AgN_x sites) contribute in a considerable lower extent to the overall catalytic activity.

In the presence of a monometallic Ag-based catalyst (Ag@CN-800), which is constituted by core-shell metallic nanoparticles with a narrow size distribution (5-20 nm) and by highly dispersed AgN_x species (see Figure S9 and accompanying discussion), good activity toward the formation of product **3aa** was achieved (Figure 6a) as well. However, in spite of the smaller particle size (and therefore higher specific surface area to interact with the reactants), catalyst Ag@CN-800 is less active than the heterobimetallic one AgCr@CN-800 for the investigated reaction. This result unambiguously corroborates that the presence of chromium-derived species in catalyst AgCr@CN-800 boosts its catalytic activity.

When the monometallic catalyst Ag@CN-800 was leached with acid to remove the metallic Ag nanoparticles, and the resulting material (Ag@CN-800-Acid) only containing highly dispersed Ag-N_x sites (see Figure S10 and accompanying discussion) was used as a catalyst under otherwise the same conditions, a decrease of the selectivity toward the coupling product **3aa** was observed as the conversion increases (Figure 6c). Similarly, the use of catalyst Cr@CN-800-Acid, which is constituted by the same Cr species (i.e. CrN and highly dispersed Cr-N_x sites) than catalyst

AgCr@CN-800-Acid but in the absence of Ag-N_x species (see Figure S11 and accompanying discussion), led to the same loss of selectivity as well (Figure 6d).

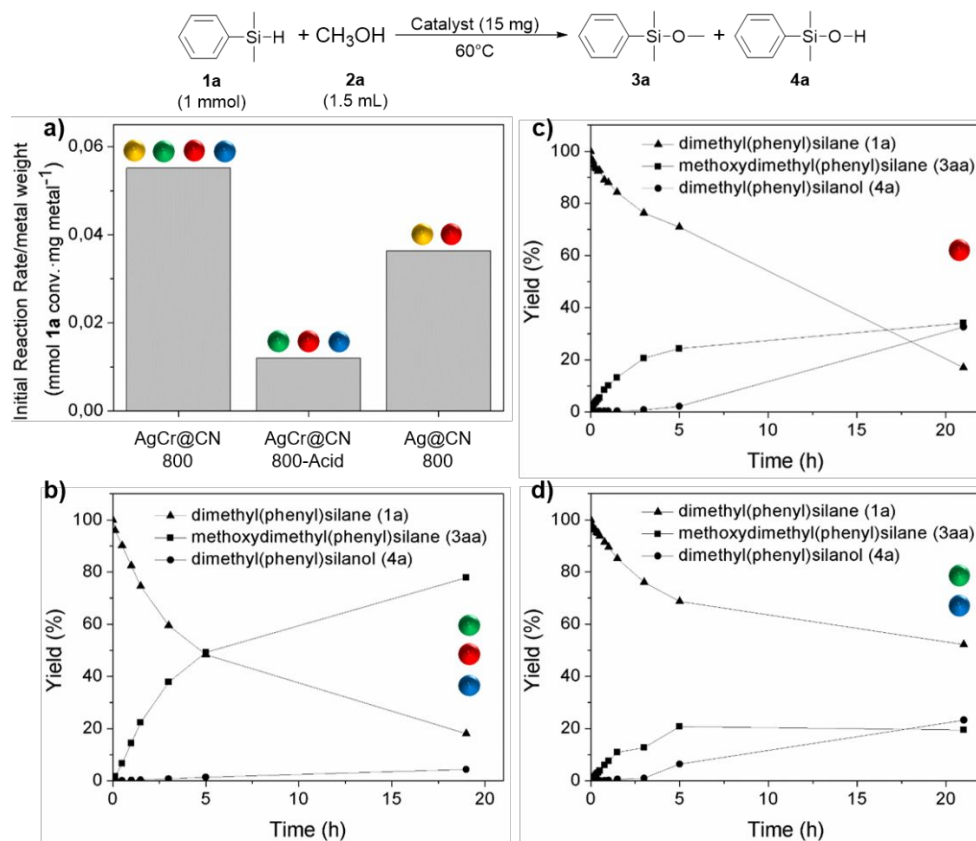


Figure 6. (a) Comparison of the metal mass activity for catalysts AgCr@CN-800, AgCr@CN-800-Acid and Ag@CN-800 in the dehydrogenative coupling reaction of **1a** with methanol (**2a**). Concentration/time diagram for catalyst AgCr@CN-800-Acid (b), Ag@CN-800-Acid (c), and Cr@CN-800-Acid (d). Reaction conditions: **1a** (1 mmol), **2a** (1.5 mL), catalyst (15 mg), 60 °C. Colored dots represent which active species are present in the catalyst used: Ag particles (yellow), CrN particles (green), AgN_x sites (red), and CrN_x sites (blue).

Overall, the above comparative catalytic study reveals that Ag particles are the most active species and that their activity is boosted by the presence of Cr-derived species. In the absence of Ag

particles, the rest of metal species (i.e. CrN particles as well as highly dispersed Ag-N_x and Cr-N_x sites) cooperatively catalyze this reaction with a slower reaction rate but with high selectivity. However, a considerably loss of selectivity is achieved when the catalyst only comprises either Ag-N_x sites or Cr-derived species (i.e. CrN particles and Cr-N_x sites), further supporting the synergistic role of Ag- and Cr-derived species in catalyst AgCr@CN-800.

Kinetic and *in-situ* Raman spectroscopy investigations

To get insights into the reaction pathway for the dehydrogenative coupling of silanes with alcohols in the presence of catalyst AgCr@CN-800, kinetic experiments at 30 °C under air conditions were performed by measuring initial reaction rates at variable concentrations of

the silane **1a** or methanol (**2a**) while keeping constant the other reactant. The initial reaction rate for the generation of **3aa** was proportional to the concentration of methanol, but a decrease was observed when increasing the amount of the silane (Figure S12).

According to Hougen–Watson/Langmuir–Hinshelwood principles, developed for describing reaction mechanisms occurring on the surface of heterogeneous catalysts, these observations suggest that the alcohol activation is the rate-determining step, and that both reactants, i.e. the silane and the alcohol, compete by the same active sites.¹⁹⁸⁻

²⁰¹ Furthermore, a kinetic isotope effect ($k_H/k_D = 2.45$) was observed when using O-

deuterated methanol (CH_3OD) as reactant, further confirming that the activation of the O-H bond is involved in the slowest reaction step.

As commented above, the presence of O_2 is crucial to accomplish the dehydrogenative coupling reaction and higher catalytic activity was obtained in the presence of catalyst AgCr@CN-800 in comparison with the Cr-free catalyst (Ag@CN-800). Thus, with the aim of getting more clues into the reaction mechanism, we first performed Raman studies of oxygen activation, revealing that catalyst AgCr@CN-800 displays a higher ability to activate oxygen than catalyst Ag@CN-800 (Figure 7a). Apart from the G- (1570 cm^{-1}), D- (1350 cm^{-1}) and 2D- ($2500\text{-}2800\text{ cm}^{-1}$) bands (Figure S13), characteristic of the formation of graphitic carbon with some degree of defect sites, the recorded spectra for both catalysts display different Raman bands as consequence of a markedly different reactivity toward O_2 activation. The Raman spectrum of catalyst AgCr@CN-800 exhibits intense bands at 613 cm^{-1} corresponding to subsurface atomic oxygen species (labelled as O_β), and at 801 and 350 cm^{-1} associated with the stretching and bending vibration of chemisorbed surface atomic oxygen species (denoted as O_γ).²⁰²⁻²⁰⁴ In the opposite, in catalyst Ag@CN-800 weakly activated molecular O_2 is predominately observed (Raman bands at 911 and 1012 cm^{-1}

1
2
3
4 ¹)^{203, 205} together with weakly adsorbed atomic oxygen species at 479 cm⁻¹ (denoted as
5
6
7 O_α). According to previous studies on Ag-based catalysts, the different reactivity toward
8
9
10 oxygen activation observed between both catalysts could arise from structural defects
11
12
13 and/or electronic properties modification in the Ag particles likely provoked in catalyst
14
15
16 AgCr@CN-800 by the presence of Cr species, which are in intimate contact with the Ag
17
18
19
20
21 particles, as revealed by electron microscopy characterization.
22
23

24
25 In order to unravel the role of the surface oxygen species on the reaction mechanism,
26
27
28 “*in-situ*” Raman experiments in the presence of catalyst AgCr@CN-800 were undertaken.
29
30
31 After dosing methanol on a pre-oxidized catalyst, new Raman bands associated to
32
33
34 hydroxyl (575 cm⁻¹) and alkoxy (ν(C-O) at 1013 cm⁻¹) species emerged concomitant with
35
36
37 the depletion of the bands at 801 cm⁻¹ associated with the surface O_γ species (Figure 7b).
38
39
40
41 A similar depletion behaviour of these species was also observed after silane dosing on
42
43
44 the pre-oxidized catalyst in the absence of methanol (Figure S14a), further confirming
45
46
47 that both reactants, i.e. the silane and the alcohol, compete by the same active sites, as
48
49
50 revealed the kinetic study. It should be mentioned that the reactivity observed for the
51
52
53 surface O_γ species is in line with other studies in the literature where they have been
54
55
56
57
58
59
60

reported as active centres for silane²⁰⁶⁻²⁰⁹ and methanol²⁰⁴ oxidation reactions. Interestingly, no O-H bond activation of methanol was observed in a non-oxidized catalyst surface (Figure S14b). This result agrees not only with the fact that no reaction took place under an inert atmosphere, but also with the higher reaction rate observed by bubbling pure O₂ gas into the reaction, which agrees with the kinetic findings where methanol activation was found to be the rate-limiting step.

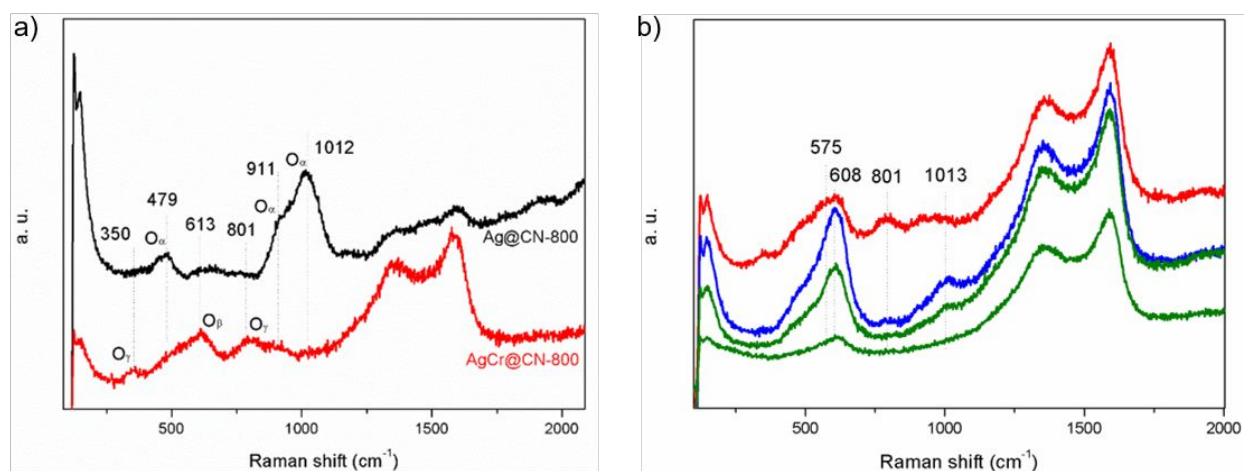
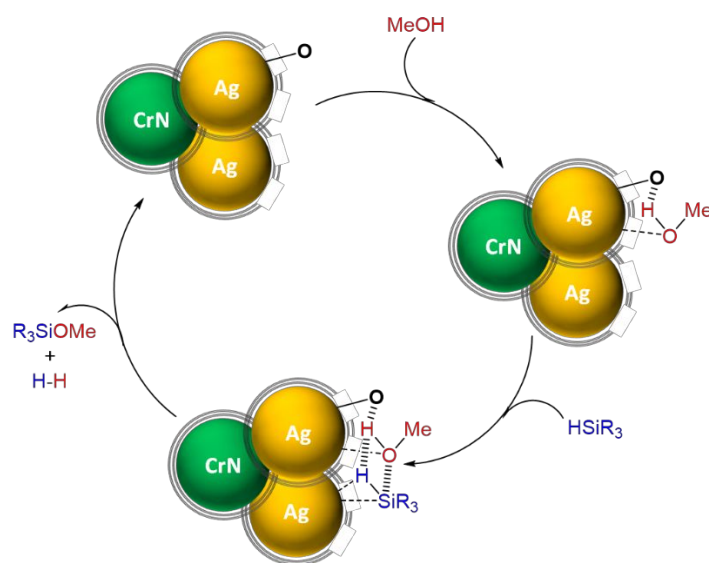


Figure 7. (a) Evolution of the bands in the Raman spectra on catalysts AgCr@CN-800 (red line) and Ag@CN-800 (black line) in a 20% O₂/Ar flow at room temperature. (b) Evolution of the bands in the Raman spectra on catalyst AgCr@CN-800 after sequentially dosing at room temperature a 20% O₂/Ar flow (red line), a methanol/Ar flow (blue line), and a silane **1a**/Ar flow (green lines).

Next, the reactivity of the pre-formed methoxy (-OCH₃) and hydroxyl (-OH) species was investigated after silane feeding. As shown in Figure 7b, the methoxy species (1012 cm⁻¹) rapidly disappeared in the presence of the silane together with a decrease in the intensity of the band associated to hydroxyl and subsurface oxygen species (575-613 cm⁻¹), thus indicating that reaction between activated methanol and the silane to form the silyl ether **3aa** and H₂ was accomplished. The fact that the silanol (**4a**) and disiloxane (**5a**) compounds were detected as by-products in the macro-kinetic studies agrees with the herein observed progressive depletion of the Raman bands at 613 and 801 cm⁻¹ associated with subsurface O_β and surface O_γ species, respectively, by further reaction of these species with the silane.



Scheme 2. Proposed mechanism for the oxygen-assisted dehydrogenative coupling reaction of silanes with alcohols in the presence of catalyst AgCr@CN-800.

Based on these results, a plausible mechanism for the dehydrogenative coupling of silanes with alcohols in the presence of catalyst AgCr@CN-800 is proposed (Scheme 2).

Oxygen activated Ag surface species act as Brønsted base sites producing hydroxyl and alkoxy species by reaction with the alcohol. No direct evidence on the silane activation on the catalyst surface were obtained likely because of it is a fast step of the overall catalytic reaction. However, considering the well-established reactivity of silanes with metals, the activation could take place through the formation of a silyl-metal hydride intermediate by Si-H bond insertion into the Ag surface.²⁰⁶ Subsequently, the nucleophilic attack of the alkoxy species derived from the alcohol to the electrophilic Si atom of the silyl-metal hydride intermediate would generate the corresponding silyl ether and molecular H₂ as well as the recovering of the oxygen activated Ag surface species. It should be noted that, accordingly to the work of Belkova, Shubina and co-workers,²¹⁰ the silane activation could also be accounted by coordination of the previously formed alkoxide ionic species yielding hypervalent pentacoordinate silicon complexes,²¹¹⁻²¹³

which enable the formation of dihydrogen bonded (MeO) $_3$ SiH...HOMe species making straightforward the proton-hydride transfer and H $_2$ formation.

Reusability of catalyst AgCr@CN-800

In order to investigate the recyclability of catalyst AgCr@CN-800, the model reaction between the silane **1a** and methanol was scaled-up by the factor of seven for practical reasons. After each catalytic run, the catalyst was separated from the reaction mixture, washed with ethyl acetate and diethyl ether, and reused without any reactivation treatment. ICP-MS analysis of the reaction filtrate after each run revealed that the metal (Ag and Cr) content was below the detection limit, thus confirming that no significant metal leaching occurred. Moreover, when the catalyst was removed from the reaction mixture by filtration at 51 % yield of **3aa** the reaction did not proceed any further (Figure S15).

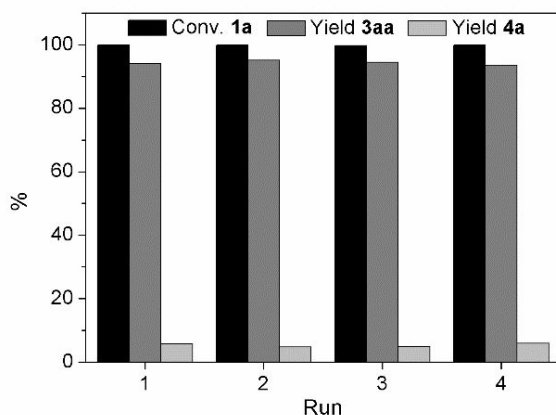


Figure 8. Recycling of catalyst AgCr@CN-800 for the dehydrogenative coupling reaction of **1a** with methanol. Reaction conditions: **1a** (7 mmol), **2a** (10.5 mL), catalyst AgCr@CN-800 (105 mg), 30 °C, 75 min (run 1), 90 min (run 2) 135 min (run 3) or 180 min (run 4). Conversions and yields determined by GC using anisole as an internal standard (380 μ L, 3.5 mmol).

After the fourth run, the morphology of the catalyst was investigated by TEM and EDS elemental mapping (Figure S16). Metal particles were still covered by a few layers of N-doped graphitic carbon shell and good dispersion of all elements (C, N, Ag and Cr) overlapping to each other in spatial locations could also be observed. Furthermore, no significant changes were detected by XRD and XPS analysis (Figure S17). The stability of catalyst AgCr@CN-800, suggested by the characterization results, was further confirmed by the excellent yields of the silyl product **3aa** obtained after each catalytic run with only a slight decrease of the reaction rate, which could be overcome by prolonging the reaction time (Figure 8).

Reaction scope of catalyst AgCr@CN-800

The catalytic performance of catalyst AgCr@CN-800 was further explored for the dehydrogenative coupling of various silanes with different alcohols. As shown in Table 1, excellent selectivity to the corresponding alkoxysilane products (**3ab-ag**) was achieved in the reaction between dimethylphenylsilane (**1a**) and alcohols (**2b-g**) with longer alkyl chain length, including linear and branched ones. (Table 1, entries 1-7). Comparing to methanol, longer reaction times were needed for full (or high) conversions, most likely because of steric effects. Benzyl alcohol (**2h**) also reacted efficiently at higher temperature (100 °C) with silane **1a** affording the desired silyl ether product (**3ah**) in 91

% selectivity (Table 1, entry 8). Interestingly, when the reaction was performed in the presence of ethylene glycol, the silyloxy(ethan-1-ol) product (**3ai**) was afforded with high selectivity (Table 1, entry 9). Besides silane **1a**, triphenyl- (**1b**), diphenyl- (**1c**), and phenylsilane (**1d**) were also excellent candidates to accomplish the dehydrogenative coupling reaction with different alcohols in the presence of catalyst AgCr@CN-800 to the corresponding mono- (**3ba**), di- (**3ca**, **3cc**, **3cd**), and trialkoxysilane (**3da**) products with good to excellent selectivity (Table 1, entries 10-14). In general, the discrete loss of selectivity is associated with the formation of the corresponding silanol, disiloxane and/or siloxane oligomer products by reaction of silanes with oxygen activated Ag surface species and/or with ubiquitous water present in alcohols.

Table 1 Dehydrogenative coupling of silanes and alcohols catalyzed by AgCr@CN-800^a

Entry	Silane	Alcohol	Time [min]	Conversion ^b [%]	Selectivity to 3 ^b [%]
1 ^c	Me ₂ PhSiH (1a)	MeOH (2a)	20	>99	97 (89) ^d
2	Me ₂ PhSiH (1a)	EtOH (2b)	60	>99	93
3 ^c	Me ₂ PhSiH (1a)	<i>n</i> -PrOH (2c)	60	>99	94
4 ^e	Me ₂ PhSiH (1a)	<i>n</i> -BuOH (2d)	180	96	96
5 ^{c, e}	Me ₂ PhSiH (1a)	<i>n</i> -HexOH (2e)	60	97	96
6 ^e	Me ₂ PhSiH (1a)	<i>i</i> -PrOH (2f)	60	99	85
7	Me ₂ PhSiH (1a)	<i>sec</i> -BuOH (2g)	360	99	89
8 ^{e, f}	Me ₂ PhSiH (1a)	BzOH (2h)	120	95	95
9	Me ₂ PhSiH (1a)	HOEtOH (2i)	60	>99	(79)

10 ^c	Ph ₃ SiH (1b)	MeOH (2a)	60	95	(93)
11 ^c	Ph ₂ SiH ₂ (1c)	MeOH (2a)	45	99	89
12	Ph ₂ SiH ₂ (1c)	<i>n</i> -PrOH (2c)	45	99	(92)
13	Ph ₂ SiH ₂ (1c)	<i>n</i> -BuOH (2d)	60	99	(80)
14 ^{c, g}	PhSiH ₃ (1d)	MeOH (2a)	20	99	89

^aReaction conditions: silane (1 mmol), alcohol (1.5 mL), AgCr@CN-800 (15 mg), 60 °C.

^bDetermined by GC using anisole (54 µL, 0.5 mmol) as an internal standard. Yield of isolated products in parentheses. ^cAnhydrous alcohol as reactant. ^dIsolated yield on a gram-scale reaction: **1a** (1 g), MeOH (11 mL), AgCr@CN-800 (110 mg), 30 °C, 75 min. ^eAgCr@CN-800 (30 mg).

^f100 °C. ^gAgCr@CN-800 (5 mg).

CONCLUSIONS

We have developed a series of N-doped carbonaceous heterobimetallic nanostructured materials prepared by pyrolysis of chitosan at different temperatures in the presence of highly dispersed Ag₂CrO₄. Their catalytic potential has been investigated for the dehydrogenative coupling reaction of various silanes with different alcohols. The most active catalyst AgCr@CN-800 catalyzes this reaction under aerobic and mild conditions, even at 0 °C, affording the corresponding silyl ether products with excellent selectivity. Furthermore, the catalyst displays good stability and recyclability.

Characterization results revealed that catalyst AgCr@CN-800 comprises Ag and CrN aggregated particles, as well as highly dispersed Ag-N_x and Cr-N_x sites embedded in N-doped graphitic structures. The rational design of structure-related catalysts in combination with acid-leaching treatments allowed for carrying out catalytic control experiments, which revealed that the most active species are the Ag particles and that their activity is boosted by the presence of Cr-derived species. It has been demonstrated by *in-situ* Raman spectroscopy that this boosting effect

1
2
3 is related with a higher ability for the generation of oxygen activated surface species, which has
4
5
6 resulted to play a crucial role as Brønsted base sites for the dissociative activation of the alcohol
7
8
9 that is the rate-determining step of the whole process.
10

11 This work not only provides solid evidences of a catalyst involving surface oxygen activated
12
13 species as key active sites for environmentally benign reactions for green organic synthesis, but
14
15 also offers insights for disentangling the heterogeneous composition of chitosan-derived annealed
16
17 materials containing metals.
18
19
20

21 22 **EXPERIMENTAL SECTION** 23

24 25 **Reagents** 26

27
28 Ag_2CrO_4 was synthesized according to the co-precipitation method previously reported in
29
30
31 the literature.²¹⁴ $\alpha\text{-Ag}_2\text{WO}_4$ and $\alpha\text{-AgVO}_3$ were prepared according to literature methods
32
33
34 as well.²¹⁵⁻²¹⁶ Chitosan, silanes and alcohols, including anhydrous methanol, were
35
36
37
38 obtained from commercial sources (Sigma Aldrich) and were used as received, while *n*-
39
40
41 propanol and *n*-hexanol were dried over molecular sieves prior to be used.
42
43
44
45

46 47 **Synthesis of catalysts AgCr@CN** 48

49 In a 250 mL beaker, Ag_2CrO_4 (0.074 g) and chitosan (0.926 g) were dispersed by
50
51
52 sonication in 30 mL of ethanol for 20 min. Then, the solvent was evaporated under
53
54
55
56
57
58
59
60

1
2
3 atmospheric pressure and stirring conditions at 70 °C, and the residue was dried
4
5
6
7 overnight at this temperature under high vacuum. The dried sample was transferred into
8
9
10 a quartz tube, and pyrolyzed at temperatures between 400-900 °C for 2 h in a vertical
11
12
13 tubular oven with a ramp rate of 10 °C/min while flushing N₂ through the tube constantly
14
15
16
17 until the oven was cooled down to room temperature. The resulting material was ground
18
19
20 in an agate mortar and stored in an Eppendorf under air. Catalyst M-free@CN was
21
22
23 prepared by directly pyrolyzing chitosan (1 g) under the same annealing treatment,
24
25
26
27 followed by grinding in an agate mortar.
28
29
30
31

32 **Synthesis of AgW@CN-800 and AgV@CN-800**

33
34

35 The preparation of catalysts AgW@CN-800 and AgV@CN-800 was carried following
36
37
38 the same procedure to the one described for AgCr@CN materials. 0.070 g of α -Ag₂WO₄
39
40
41 or 0.078 g of α -AgVO₃, and 0.930 g or 0.922 g of chitosan, respectively, were used as
42
43
44 precursors. The other experimental procedures were the same, and the pyrolysis
45
46
47
48 temperature was 800 °C.
49
50
51
52

53 **Preparation of catalyst AgCr@CN-800-Acid**

54
55
56
57
58
59
60

AgCr@CN-800-Acid was prepared by acid leaching of AgCr@CN-800. In a 100 mL beaker, 200 mg of catalyst AgCr@CN-800 were dispersed in a 0.5 mol/L H₂SO₄ aqueous solution (50 mL) under stirring conditions and heated at 75 °C for 6 h. After that, the resulting material was recovered by centrifugation, washed twice with water, twice with ethanol and dried at 60 °C overnight.

Synthesis of Ag@CN-800

Chitosan (0.924 g) was dispersed by sonication for 20 min in an ethanol solution of AgNO₃ (0.076 g in 30 mL). The other experimental procedures were the same the ones described for AgCr@CN materials, and the pyrolysis temperature was 800 °C.

Synthesis of Ag@CN-800-Acid

Ag@CN-800-Acid was prepared by five consecutive acid leaching treatments starting from 240 mg of catalyst Ag@CN-800. After each treatment, the resulting material was recovered by centrifugation, washed twice with water, twice with ethanol, dried at 60 °C, and used for the next one. The first three acid leaching treatments were carried out in a 100 mL beaker, in which the catalyst was dispersed in a 1, 2 or 4 mol/L H₂SO₄ aqueous solution (50 mL), respectively, under stirring conditions and heated at 75 °C for 16 h. The last two acid leaching treatments were performed in a 100 mL Teflon vessel containing a stirring bar. Once the materials were dispersed

1
2
3 in a 4 mol/L H₂SO₄ aqueous solution (50 mL), the Teflon vessel was sealed and heated at 120 or
4
5 140 °C, respectively, under stirring conditions for 2 h with a heating rate of 5 °C/min in a
6
7 microwave equipment using an irradiation power of maximum 800 W.
8
9

10 11 **Synthesis of Cr@CN-800-Acid** 12 13

14
15 Chitosan (0.957 g) was dispersed by sonication for 20 min in an ethanol solution of K₂CrO₄
16
17 (0.043 g in 30 mL). Afterward, the solvent was evaporated under atmospheric pressure and stirring
18
19 conditions at 70 °C, and the residue was dried overnight at this temperature under a high *vacuum*.
20
21 Then, the dried sample was transferred into a quartz tube, and pyrolyzed at 800 °C for 2 h in a
22
23 vertical tubular oven with a ramp rate of 10 °C/min while flushing N₂ through the tube constantly
24
25 until the oven was cooled down to room temperature again. The resulting material was ground in
26
27 an agate mortar and transferred to a 100 mL beaker containing a stirring bar where it was dispersed
28
29 in a 1 mol/L H₂SO₄ aqueous solution (50 mL) under stirring conditions and heated at 75 °C for 16
30
31 h. This material was recovered by centrifugation, washed twice with water, twice with ethanol,
32
33 and dried at 60 °C.
34
35
36
37
38

39 **Characterizations** 40 41

42
43 Powder X-ray diffraction (XRD) measurements were performed in a D/MAX-2500 PC
44
45 diffractometer (Rigaku) with Cu K α radiation (λ = 1.5406 Å). Samples for electron microscopy
46
47 studies were prepared by sprinkling the material directly onto the holey-carbon-coated nickel or
48
49 copper grids. Some of the measurements were performed in a JEM 2100F microscope operating
50
51 at 200 kV both in transmission (TEM) and in scanning-transmission modes (STEM). C_s-corrected
52
53 Scanning Transmission Electron Microscopy (STEM) measurements were performed in a probe
54
55
56
57
58
59
60

corrector Titan Themis operated at 300 kV. X-ray photoelectron spectra were acquired with a monochromatic Al K α X-ray source (1486.6 eV) using a pass energy of 20 eV on a Kratos AXIS ultra DLD spectrometer. The C1s peak at 284.6 eV was used to provide a precise energy calibration. The metal content in catalysts was determined by inductively coupled plasma mass spectrometry (ICP-MS) using an ICP-MS Agilent 7500 CX spectrometer. Samples for ICP-MS analysis were previously digested in a microwave equipment (CEM Corp, Matthews, NC) equipped with a temperature controller (MARS6 iWave). A previously weighted amount of material and 10 mL HNO₃ (65 % p/p) were introduced in a 100 mL Teflon vessel, sealed and heated at 210 °C under static conditions for 25 min with a heating rate of 12 °C/min by irradiating at a maximum power of 1800 W. After cooling down to room temperature, the resulting solution was transferred to a previously tared 25 mL-volumetric flask and diluted with MiliQ H₂O.

¹H-NMR spectra of isolated products were recorded on a Bruker AV 300 spectrometer. All chemical shifts (δ) are reported in parts per million (ppm) and coupling constants (J) in Hz. For ¹H-NMR and ²⁹Si-NMR chemical shifts are reported relative to tetramethylsilane (δ 0.0 ppm in CDCl₃) or *d*-solvent peaks (δ 77.16 ppm CDCl₃) for ¹³C-NMR. GC analyses were obtained on a Shimadzu GC-2010 apparatus equipped with a FID and a Technokroma (TBR-5MS, 30 m x 0.25 mm x 0.25 μ m) column. GC-Mass characterization was carried out on a GC-Mass Agilent 6890 Network equipped with a capillary column Agilent (HP-5, 30 m x 0.32 mm x 0.25 μ m) and a mass-selective detector. The unambiguously detection of the H₂ evolved from the reaction was carried out using an Agilent 490 MicroGC equipped with two columns (Pore Plot Q and MolSieve 5A) and one thermal conductivity detector (TCD).

Raman spectra were recorded at room temperature using a 514 nm laser excitation on a Renishaw Raman spectrometer (“in via”) equipped with a CCD detector. The laser power on the sample was

1
2
3 10-50 mW and a total of 20 acquisitions (10 s exposure time) were taken for each spectrum.
4
5 Analyses on different positions of the sample were recorded (spectral resolution 2 μ m).
6
7 Measurements were carried out using a home-made cell, where the catalyst powder was introduced
8
9 without any previous treatment.
10
11
12

13 **General procedure for the catalytic dehydrogenative coupling of silanes and alcohols**

14
15
16
17 Catalytic experiments were performed under aerobic conditions in a 50 mL round-bottom flask
18
19 equipped with a reflux condenser and a magnetic stirring bar. Once the catalyst (15 mg) and the
20
21 alcohol (1.5 mL) were introduced, the reaction flask was heated at 60 °C and let equilibrate for 5
22
23 min. Then, the silane (1 mmol) and anisole (54 μ L, 0.5 mmol) as an internal standard were added,
24
25 setting this point as the starting time of the reaction. Yields and conversions were determined by
26
27 GC analysis taking samples from the reaction mixture at the reported times. No internal standard
28
29 was added in reactions from which isolated yields were calculated. After reaction completion and
30
31 dilution with ethyl acetate, the catalyst was separated off by filtration, and the solvent was removed
32
33 under reduced pressure. Some of the products were purified by flash-column chromatography
34
35 using *n*-hexane as an eluent phase (see the Supporting Information). For the recycling experiments,
36
37 the general procedure was scaled up by the factor of 7, and the reaction was performed at 30 °C in
38
39 an opened 50 ml centrifugation tube. After reaction completion, the reaction mixture was diluted
40
41 with ethyl acetate, and the catalyst was separated off by centrifugation, cleaned with ethyl acetate,
42
43 diethyl ether, and dried at 60 °C for 30 min before using for the next run again.
44
45
46
47
48
49

50 **ASSOCIATED CONTENT**

51
52
53
54
55
56
57
58
59
60

The Supporting Information is available free of charge via the Internet at

<http://pubs.acs.org>.

Extended data for the characterization of catalysts, additional catalytic and Raman spectroscopic experiments, and characterization data of isolated products.

Notes

The authors declare no competing financial interest.

ACKNOWLEDGMENT

The authors thank the financial support from MICIU/AEI/FEDER (PGC2018-094417-B-I00 and RTI2018-098237-B-C22) and Universitat Jaume I (UJI-A2019-16, UJI-B2019-30, and UJI-B2018-23). I. S. thanks the Spanish Ministerio de Economía, Industria y Competitividad (MINECO) for a postdoctoral “Juan de la Cierva-Incorporación” fellowship (IJCI-2016-30590), and the financial support from the “José Castillejo” Mobility Program (CAS19/00339) of the Ministerio de Ciencia, Innovación y Universidades (MICIU). S. M. acknowledges DGA/fondos FEDER (construyendo Europa desde Aragón) for funding the research group Platón (E31_17R). D. V-E. thanks the MICIU for a FPU grant

(FPU15/03011). E. L. and M. A. thank the financial support from FAPESP (2013/07296-2), CNPq (166281/2017-4), CAPES, and FINEP. The authors also thank the “Servei Central d’Instrumentació Científica (SCIC)” of the Universitat Jaume I, as well as Dr. G. Antorrena for technical support in XPS studies.

REFERENCES

1. Wuts, P. G. M.; Green, T. W., *in Greene's Protective Groups in Organic Synthesis*. 4th ed.; Wiley-Interscience: New Jersey, 2006.
2. Denmark, S. E.; Liu, J. H. C., Silicon-Based Cross-Coupling Reactions in the Total Synthesis of Natural Products. *Angew. Chem. Int. Ed.* **2010**, *49* (17), 2978-2986.
3. Crouch, R. D., Recent Advances in Silyl Protection of Alcohols. *Synth. Commun.* **2013**, *43* (17), 2265-2279.
4. Schuppe, A. W.; Newhouse, T. R., Assembly of the Limonoid Architecture by a Divergent Approach: Total Synthesis of (±)-Andirolide N via (±)-8α-Hydroxycarapin. *J. Am. Chem. Soc.* **2017**, *139* (2), 631-634.
5. Smith, M. B., *in Organic Synthesis*. 4th ed.; Academic Press: Boston, 2017.

6. Osterholtz, F. D.; Pohl, E. R., Kinetics of the hydrolysis and condensation of organofunctional alkoxysilanes: a review. *J. Adhes. Sci. Technol.* **1992**, *6*(1), 127-149.
7. Belelli, P. G.; Ferreira, M. L.; Damiani, D. E., A theoretical and experimental study of the possible phenyltriethoxysilane species found on treated silica. *J. Mol. Catal. A: Chem.* **2000**, *159*(2), 315-325.
8. Díaz, I.; Pérez-Pariente, J., Synthesis of Spongelike Functionalized MCM-41 Materials from Gels Containing Amino Acids. *Chem. Mater.* **2002**, *14* (11), 4641-4646.
9. Matheron, M.; Gacoin, T.; Boilot, J. P.; Bourgeois, A.; Brunet-Bruneau, A.; Rivory, J.; Jimenez, A.; Biteau, J., Ordered mesoporous organosilica films. In *Stud. Surf. Sci. Catal.*, Sayari, A.; Jaroniec, M., Eds. Elsevier: 2005; Vol. 156, pp 327-334.
10. Shimojima, A.; Kuroda, K., Controlled synthesis of nanostructured silica-based materials from designed alkoxysilanes. *J. Sol-Gel Sci. Technol.* **2008**, *46*(3), 307-311.

11. Zhou, Q.; Yan, S.; Han, C. C.; Xie, P.; Zhang, R., Promising Functional Materials Based on Ladder Polysiloxanes. *Adv. Mater.* **2008**, *20* (15), 2970-2976.
12. Carrillo, A. I.; García-Martínez, J.; Llusar, R.; Serrano, E.; Sorribes, I.; Vicent, C.; Alejandro Vidal-Moya, J., Incorporation of cubane-type Mo₃S₄ molybdenum cluster sulfides in the framework of mesoporous silica. *Microporous Mesoporous Mater.* **2012**, *151*, 380-389.
13. Kamino, B. A.; Bender, T. P., The use of siloxanes, silsesquioxanes, and silicones in organic semiconducting materials. *Chem. Soc. Rev.* **2013**, *42* (12), 5119-5130.
14. Gómez-Avilés, A.; Aranda, P.; Fernandes, F. M.; Belver, C.; Ruiz-Hitzky, E., Silica-Sepiolite Nanoarchitectures. *J. Nanosci. Nanotechnol.* **2013**, *13* (4), 2897-2907.
15. Negrete; Letoffe, J.-M.; Putaux, J.-L.; David, L.; Bourgeat-Lami, E., Aqueous Dispersions of Silane-Functionalized Laponite Clay Platelets. A First Step toward the Elaboration of Water-Based Polymer/Clay Nanocomposites. *Langmuir* **2004**, *20* (5), 1564-1571.
16. Jaber, M.; Gaslain, F. O. M.; Miehe-Brendlé, J., Rapid and direct synthesis of spherical organotalc. *Clays Clay Miner.* **2009**, *57* (1), 35-39.

- 1
2
3
4 17. Corey, E. J.; Venkateswarlu, A., Protection of hydroxyl groups as tert-
5
6
7 butyldimethylsilyl derivatives. *J. Am. Chem. Soc.* **1972**, *94* (17), 6190-6191.
8
9
10
11 18. Chaudhary, S. K.; Hernandez, O., 4-dimethylaminopyridine: an efficient and
12
13
14 selective catalyst for the silylation of alcohols. *Tetrahedron Lett.* **1979**, *20* (2), 99-
15
16
17 102.
18
19
20
21 19. Kim, S.; Chang, H., 1,1,3,3-Tetramethylguanidine: An Effective Catalyst for the t-
22
23
24 Butyldimethylsilylation of Alcohols. *Synth. Commun.* **1984**, *14* (10), 899-904.
25
26
27
28 20. Patschinski, P.; Zhang, C.; Zipse, H., The Lewis Base-Catalyzed Silylation of
29
30
31 Alcohols—A Mechanistic Analysis. *J. Org. Chem.* **2014**, *79* (17), 8348-8357.
32
33
34
35 21. Melen, R. L., Dehydrocoupling routes to element–element bonds catalysed by
36
37
38 main group compounds. *Chem. Soc. Rev.* **2016**, *45* (4), 775-788.
39
40
41
42 22. Kuciński, K.; Hreczycho, G., Catalytic Formation of Silicon–Heteroatom (N, P, O,
43
44
45 S) Bonds. *ChemCatChem* **2017**, *9* (11), 1868-1885.
46
47
48
49 23. Ventura-Espinosa, D.; Carretero-Cerdán, A.; Baya, M.; García, H.; Mata, J. A.,
50
51
52 Catalytic Dehydrogenative Coupling of Hydrosilanes with Alcohols for the
53
54
55
56
57
58
59
60

- 1
2
3
4 Production of Hydrogen On-demand: Application of a Silane/Alcohol Pair as a
5
6
7 Liquid Organic Hydrogen Carrier. *Chem. Eur. J.* **2017**, *23* (45), 10815-10821.
8
9
- 10 24. Ventura-Espinosa, D.; Sabater, S.; Carretero-Cerdán, A.; Baya, M.; Mata, J. A.,
11
12
13 High Production of Hydrogen on Demand from Silanes Catalyzed by Iridium
14
15
16
17 Complexes as a Versatile Hydrogen Storage System. *Acs Catal.* **2018**, *8* (3), 2558-
18
19
20
21 2566.
22
23
- 24 25. Rendler, S.; Auer, G.; Oestreich, M., Kinetic Resolution of Chiral Secondary
25
26
27
28 Alcohols by Dehydrogenative Coupling with Recyclable Silicon-Stereogenic
29
30
31
32 Silanes. *Angew. Chem. Int. Ed.* **2005**, *44* (46), 7620-7624.
33
34
- 35 26. Corbin, R. A.; Ison, E. A.; Abu-Omar, M. M., Catalysis by cationic oxorhenium(v):
36
37
38
39 hydrolysis and alcoholysis of organic silanes. *Dalton Trans.* **2009**, (15), 2850-
40
41
42 2855.
43
44
- 45 27. Peterson, E.; Khalimon, A. Y.; Sirnionescu, R.; Kuzmina, L. G.; Howard, J. A. K.;
46
47
48
49 Nikonov, G. I., Diversity of Catalysis by an Imido-Hydrido Complex of Molybdenum.
50
51
52
53 Mechanism of Carbonyl Hydrosilylation and Silane Alcoholysis. *J. Am. Chem. Soc.*
54
55
56 **2009**, *131* (3), 908-+.
57
58
59
60

- 1
2
3
4 28. Mukherjee, D.; Thompson, R. R.; Ellern, A.; Sadow, A. D., Coordinatively
5
6
7 Saturated Tris(oxazolinyl)borato Zinc Hydride-Catalyzed Cross Dehydrocoupling
8
9
10 of Silanes and Alcohols. *Acs Catal.* **2011**, *1* (7), 698-702.
11
12
13
14 29. Sattler, W.; Parkin, G., Zinc Catalysts for On-Demand Hydrogen Generation and
15
16
17 Carbon Dioxide Functionalization. *J. Am. Chem. Soc.* **2012**, *134* (42), 17462-
18
19
20
21 17465.
22
23
24 30. Garcés, K.; Fernández-Alvarez, F. J.; Polo, V.; Lalrempuia, R.; Pérez-Torrente, J.
25
26
27 J.; Oro, L. A., Iridium-Catalyzed Hydrogen Production from Hydrosilanes and
28
29
30
31 Water. *ChemCatChem* **2014**, *6* (6), 1691-1697.
32
33
34
35 31. Cardoso, J. M. S.; Lopes, R.; Royo, B., Dehydrogenative silylation of alcohols
36
37
38 catalysed by half-sandwich iron N-heterocyclic carbene complexes. *J. Organomet.*
39
40
41
42 *Chem.* **2015**, *775*, 173-177.
43
44
45 32. Vijjamarri, S.; Chidara, V. K.; Rousova, J.; Du, G., Dehydrogenative coupling of
46
47
48 alcohols and carboxylic acids with hydrosilanes catalyzed by a salen-Mn(v)
49
50
51
52 complex. *Catal. Sci. Technol.* **2016**, *6* (11), 3886-3892.
53
54
55
56
57
58
59
60

- 1
2
3
4 33. Satoh, Y.; Igarashi, M.; Sato, K.; Shimada, S., Highly Selective Synthesis of
5
6
7 Hydrosiloxanes by Au-Catalyzed Dehydrogenative Cross-Coupling Reaction of
8
9
10 Silanols with Hydrosilanes. *Acs Catal.* **2017**, *7*(3), 1836-1840.
11
12
13
14 34. Dong, X.; Weickgenannt, A.; Oestreich, M., Broad-spectrum kinetic resolution of
15
16
17 alcohols enabled by Cu-H-catalysed dehydrogenative coupling with hydrosilanes.
18
19
20
21 *Nat. Commun.* **2017**, *8*(1), 15547.
22
23
24 35. Vijjamarri, S.; Chidara, V. K.; Du, G., Versatile Manganese Catalysis for the
25
26
27 Synthesis of Poly(silylether)s from Diols and Dicarboxyls with Hydrosilanes. *ACS*
28
29
30
31 *Omega* **2017**, *2*(2), 582-591.
32
33
34 36. Pramanik, S.; Fernandes, A.; Liautard, V.; Pucheault, M.; Robert, F.; Landais, Y.,
35
36
37 Dehydrogenative Silylation of Alcohols Under Pd-Nanoparticle Catalysis. *Chem.*
38
39
40
41
42 *Eur. J.* **2019**, *25*(3), 728-732.
43
44
45 37. Morris, L. J.; Hill, M. S.; Mahon, M. F.; Manners, I.; S. McMenamy, F.; Whittell, G.
46
47
48
49 R., Heavier Alkaline-Earth Catalyzed Dehydrocoupling of Silanes and Alcohols for
50
51
52 the Synthesis of Metallo-Polysilylethers. *Chem. Eur. J.* **2020**, *26*(13), 2954-2966.
53
54
55
56
57
58
59
60

- 1
2
3
4 38. Weickgenannt, A.; Oestreich, M., Potassium tert-Butoxide-Catalyzed
5
6
7 Dehydrogenative Si-O Coupling: Reactivity Pattern and Mechanism of an
8
9
10 Underappreciated Alcohol Protection. *Chem. Asian J.* **2009**, *4* (3), 406-410.
11
12
13
14 39. Toutov, A. A.; Betz, K. N.; Haibach, M. C.; Romine, A. M.; Grubbs, R. H., Sodium
15
16
17 Hydroxide Catalyzed Dehydrocoupling of Alcohols with Hydrosilanes. *Org. Lett.*
18
19
20
21 **2016**, *18* (22), 5776-5779.
22
23
24 40. Blackwell, J. M.; Foster, K. L.; Beck, V. H.; Piers, W. E., B(C₆F₅)₃-Catalyzed
25
26
27 Silation of Alcohols: A Mild, General Method for Synthesis of Silyl Ethers. *J. Org.*
28
29
30
31 *Chem.* **1999**, *64* (13), 4887-4892.
32
33
34
35 41. Cella, J.; Rubinsztajn, S., Preparation of Polyaryloxysilanes and
36
37
38 Polyaryloxysiloxanes by B(C₆F₅)₃ Catalyzed Polyetherification of Dihydrosilanes
39
40
41 and Bis-Phenols. *Macromolecules* **2008**, *41* (19), 6965-6971.
42
43
44
45 42. Zhou, D.; Kawakami, Y., Tris(pentafluorophenyl)borane as a Superior Catalyst in
46
47
48 the Synthesis of Optically Active SiO-Containing Polymers. *Macromolecules* **2005**,
49
50
51
52 *38* (16), 6902-6908.
53
54
55
56
57
58
59
60

- 1
2
3
4 43. Kaźmierczak, J.; Lewandowski, D.; Hreczycho, G., B(C₆F₅)₃-Catalyzed
5
6
7 Dehydrocoupling of POSS Silanols with Hydrosilanes: A Metal-Free Strategy for
8
9
10 Effecting Functionalization of Silsesquioxanes. *Inorg. Chem.* **2020**, *59* (13), 9206-
11
12
13
14 9214.
15
16
17 44. Gao, D.; Cui, C., N-Heterocyclic Carbene Organocatalysts for Dehydrogenative
18
19
20 Coupling of Silanes and Hydroxyl Compounds. *Chem. Eur. J.* **2013**, *19* (34),
21
22
23
24 11143-11147.
25
26
27 45. He, L.; Weniger, F.; Neumann, H.; Beller, M., Synthesis, Characterization, and
28
29
30 Application of Metal Nanoparticles Supported on Nitrogen-Doped Carbon:
31
32
33
34 Catalysis beyond Electrochemistry. *Angew. Chem. Int. Ed.* **2016**, *55* (41), 12582-
35
36
37
38 12594.
39
40
41 46. Cao, Y.; Mao, S.; Li, M.; Chen, Y.; Wang, Y., Metal/Porous Carbon Composites for
42
43
44
45 Heterogeneous Catalysis: Old Catalysts with Improved Performance Promoted by
46
47
48
49 N-Doping. *Acs Catal.* **2017**, *7* (12), 8090-8112.
50
51
52 47. Jagadeesh, R. V.; Surkus, A.-E.; Junge, H.; Pohl, M.-M.; Radnik, J.; Rabeah, J.;
53
54
55
56 Huan, H.; Schuenemann, V.; Brueckner, A.; Beller, M., Nanoscale Fe₂O₃-Based
57
58
59
60

- Catalysts for Selective Hydrogenation of Nitroarenes to Anilines. *Science* **2013**, *342*(6162), 1073-1076.
48. Westerhaus, F. A.; Jagadeesh, R. V.; Wienhoefer, G.; Pohl, M.-M.; Radnik, J.; Surkus, A.-E.; Rabeah, J.; Junge, K.; Junge, H.; Nielsen, M.; Brueckner, A.; Beller, M., Heterogenized cobalt oxide catalysts for nitroarene reduction by pyrolysis of molecularly defined complexes. *Nat. Chem.* **2013**, *5*(6), 537-543.
49. Jagadeesh, R. V.; Junge, H.; Pohl, M.-M.; Radnik, J.; Brückner, A.; Beller, M., Selective Oxidation of Alcohols to Esters Using Heterogeneous $\text{Co}_3\text{O}_4\text{-N@C}$ Catalysts under Mild Conditions. *J. Am. Chem. Soc.* **2013**, *135*(29), 10776-10782.
50. Stemmler, T.; Surkus, A.-E.; Pohl, M.-M.; Junge, K.; Beller, M., Iron-Catalyzed Synthesis of Secondary Amines: On the Way to Green Reductive Aminations. *ChemSusChem* **2014**, *7*(11), 3012-3016.
51. Stemmler, T.; Westerhaus, F. A.; Surkus, A.-E.; Pohl, M.-M.; Junge, K.; Beller, M., General and selective reductive amination of carbonyl compounds using a core-shell structured $\text{Co}_3\text{O}_4/\text{NGr@C}$ catalyst. *Green Chem.* **2014**, *16*(10), 4535-4540.

- 1
2
3
4 52. Jagadeesh, R. V.; Junge, H.; Beller, M., Green synthesis of nitriles using non-noble
5
6
7 metal oxides-based nanocatalysts. *Nat. Commun.* **2014**, *5*(1), 4123.
8
9
10
11 53. Jagadeesh, R. V.; Natte, K.; Junge, H.; Beller, M., Nitrogen-Doped Graphene-
12
13
14 Activated Iron-Oxide-Based Nanocatalysts for Selective Transfer Hydrogenation
15
16
17 of Nitroarenes. *Acs Catal.* **2015**, *5*(3), 1526-1529.
18
19
20
21 54. Jagadeesh, R. V.; Stemmler, T.; Surkus, A.-E.; Bauer, M.; Pohl, M.-M.; Radnik, J.;
22
23
24 Junge, K.; Junge, H.; Brueckner, A.; Beller, M., Cobalt-based nanocatalysts for
25
26
27 green oxidation and hydrogenation processes. *Nat. Protoc.* **2015**, *10*(6), 916-926.
28
29
30
31 55. Jagadeesh, R. V.; Stemmler, T.; Surkus, A.-E.; Junge, H.; Junge, K.; Beller, M.,
32
33
34 Hydrogenation using iron oxide-based nanocatalysts for the synthesis of amines.
35
36
37
38 *Nat. Protoc.* **2015**, *10*(4), 548-557.
39
40
41
42 56. Jagadeesh, R. V.; Banerjee, D.; Arockiam, P. B.; Junge, H.; Junge, K.; Pohl, M.-
43
44
45 M.; Radnik, J.; Brückner, A.; Beller, M., Highly selective transfer hydrogenation of
46
47
48 functionalised nitroarenes using cobalt-based nanocatalysts. *Green Chem.* **2015**,
49
50
51
52 *17*(2), 898-902.
53
54
55
56
57
58
59
60

- 1
2
3
4 57. Jagadeesh, R. V.; Junge, H.; Beller, M., "Nanorust"-catalyzed Benign Oxidation of
5
6
7 Amines for Selective Synthesis of Nitriles. *ChemSusChem* **2015**, *8* (1), 92-96.
8
9
10 58. Westerhaus, F. A.; Sorribes, I.; Wienhöfer, G.; Junge, K.; Beller, M., Reduction of
11
12 Nitroarenes Using CO and H₂O in the Presence of a Nanostructured Cobalt
13
14 Oxide/Nitrogen-Doped Graphene (NGr) Catalyst. *Synlett* **2015**, *26* (03), 313-317.
15
16
17 59. Chen, F.; Surkus, A.-E.; He, L.; Pohl, M.-M.; Radnik, J.; Topf, C.; Junge, K.; Beller,
18
19 M., Selective Catalytic Hydrogenation of Heteroarenes with N-Graphene-Modified
20
21 Cobalt Nanoparticles (Co₃O₄-Co/NGr@α-Al₂O₃). *J. Am. Chem. Soc.* **2015**, *137*
22
23 (36), 11718-11724.
24
25
26 60. Cui, X.; Li, Y.; Bachmann, S.; Scalone, M.; Surkus, A.-E.; Junge, K.; Topf, C.;
27
28 Beller, M., Synthesis and Characterization of Iron-Nitrogen-Doped
29
30 Graphene/Core-Shell Catalysts: Efficient Oxidative Dehydrogenation of N-
31
32 Heterocycles. *J. Am. Chem. Soc.* **2015**, *137* (33), 10652-10658.
33
34
35 61. Pisiewicz, S.; Stemmler, T.; Surkus, A.-E.; Junge, K.; Beller, M., Synthesis of
36
37 Amines by Reductive Amination of Aldehydes and Ketones using Co₃O₄/NGr@C
38
39 Catalyst. *ChemCatChem* **2015**, *7* (1), 62-64.
40
41
42
43
44
45
46
47
48
49
50
51
52
53
54
55
56
57
58
59
60

- 1
2
3
4 62. Jagadeesh, R. V.; Stemmler, T.; Surkus, A.-E.; Bauer, M.; Pohl, M.-M.; Radnik, J.;
5
6
7 Junge, K.; Junge, H.; Brueckner, A.; Beller, M., Cobalt-based nanocatalysts for
8
9
10 green oxidation and hydrogenation processes (vol 10, pg 916, 2015). *Nat. Protoc.*
11
12
13
14 **2016**, *11* (1), 192-192.
15
16
17 63. Natte, K.; Jagadeesh, R. V.; Sharif, M.; Neumann, H.; Beller, M., Synthesis of
18
19
20 nitriles from amines using nanoscale Co₃O₄-based catalysts via sustainable
21
22
23 aerobic oxidation. *Org. Biomol. Chem.* **2016**, *14* (13), 3356-3359.
24
25
26
27 64. Chen, F.; Topf, C.; Radnik, J.; Kreyenschulte, C.; Lund, H.; Schneider, M.; Surkus,
28
29
30 A.-E.; He, L.; Junge, K.; Beller, M., Stable and Inert Cobalt Catalysts for Highly
31
32
33 Selective and Practical Hydrogenation of C≡N and C=O Bonds. *J. Am. Chem. Soc.*
34
35
36
37
38 **2016**, *138* (28), 8781-8788.
39
40
41 65. Cui, X.; Surkus, A.-E.; Junge, K.; Topf, C.; Radnik, J.; Kreyenschulte, C.; Beller,
42
43
44 M., Highly selective hydrogenation of arenes using nanostructured ruthenium
45
46
47
48 catalysts modified with a carbon–nitrogen matrix. *Nat. Commun.* **2016**, *7* (1),
49
50
51
52 11326.
53
54
55
56
57
58
59
60

- 1
2
3
4 66. Pisiewicz, S.; Formenti, D.; Surkus, A.-E.; Pohl, M.-M.; Radnik, J.; Junge, K.; Topf,
5
6
7 C.; Bachmann, S.; Scalone, M.; Beller, M., Synthesis of Nickel Nanoparticles with
8
9
10 N-Doped Graphene Shells for Catalytic Reduction Reactions. *Chemcatchem*
11
12
13
14 **2016**, *8*(1), 129-134.
15
16
17 67. Formenti, D.; Topf, C.; Junge, K.; Ragaini, F.; Beller, M., Fe₂O₃/NGr@C- and Co-
18
19
20 Co₃O₄/NGr@C-catalysed hydrogenation of nitroarenes under mild conditions.
21
22
23
24 *Catal. Sci. Technol.* **2016**, *6*(12), 4473-4477.
25
26
27 68. Chen, F.; Sahoo, B.; Kreyenschulte, C.; Lund, H.; Zeng, M.; He, L.; Junge, K.;
28
29
30 Beller, M., Selective cobalt nanoparticles for catalytic transfer hydrogenation of N-
31
32
33
34
35 heteroarenes. *Chem. Sci.* **2017**, *8*(9), 6239-6246.
36
37
38 69. Chen, F.; Kreyenschulte, C.; Radnik, J.; Lund, H.; Surkus, A.-E.; Junge, K.; Beller,
39
40
41
42 M., Selective Semihydrogenation of Alkynes with N-Graphitic-Modified Cobalt
43
44
45
46 Nanoparticles Supported on Silica. *Acs Catal.* **2017**, *7*(3), 1526-1532.
47
48
49 70. Natte, K.; Neumann, H.; Jagadeesh, R. V.; Beller, M., Convenient iron-catalyzed
50
51
52
53 reductive aminations without hydrogen for selective synthesis of N-methylamines.
54
55
56
57 *Nat. Commun.* **2017**, *8*(1), 1344.
58
59
60

- 1
2
3
4 71. Formenti, D.; Ferretti, F.; Topf, C.; Surkus, A.-E.; Pohl, M.-M.; Radnik, J.;
5
6
7 Schneider, M.; Junge, K.; Beller, M.; Ragaini, F., Co-based heterogeneous
8
9
10 catalysts from well-defined α -diimine complexes: Discussing the role of nitrogen.
11
12
13 *J. Catal.* **2017**, *351*, 79-89.
14
15
16
17 72. Chen, F.; Li, W.; Sahoo, B.; Kreyenschulte, C.; Agostini, G.; Lund, H.; Junge, K.;
18
19
20 Beller, M., Hydrogenation of Pyridines Using a Nitrogen-Modified Titania-
21
22
23 Supported Cobalt Catalyst. *Angew. Chem. Int. Ed.* **2018**, *57*(44), 14488-14492.
24
25
26
27 73. Sahoo, B.; Kreyenschulte, C.; Agostini, G.; Lund, H.; Bachmann, S.; Scalone, M.;
28
29
30
31 Junge, K.; Beller, M., A robust iron catalyst for the selective hydrogenation of
32
33
34 substituted (iso)quinolones. *Chem. Sci.* **2018**, *9*(42), 8134-8141.
35
36
37
38 74. Ryabchuk, P.; Agostini, G.; Pohl, M.-M.; Lund, H.; Agapova, A.; Junge, H.; Junge,
39
40
41 K.; Beller, M., Intermetallic nickel silicide nanocatalyst—A non-noble metal-based
42
43
44 general hydrogenation catalyst. *Science Advances* **2018**, *4*(6), eaat0761.
45
46
47
48 75. Fiorio, J. L.; Gonçalves, R. V.; Teixeira-Neto, E.; Ortuño, M. A.; López, N.; Rossi,
49
50
51 L. M., Accessing Frustrated Lewis Pair Chemistry through Robust Gold@N-Doped
52
53
54 Carbon for Selective Hydrogenation of Alkynes. *Acs Catal.* **2018**, *8*(4), 3516-3524.
55
56
57
58
59
60

- 1
2
3
4 76. Li, G.; Yang, H.; Zhang, H.; Qi, Z.; Chen, M.; Hu, W.; Tian, L.; Nie, R.; Huang, W.,
5
6 Encapsulation of Nonprecious Metal into Ordered Mesoporous N-Doped Carbon
7
8 for Efficient Quinoline Transfer Hydrogenation with Formic Acid. *Acs Catal.* **2018**,
9
10
11
12
13
14 *8* (9), 8396-8405.
15
16
17 77. Li, W.; Artz, J.; Broicher, C.; Junge, K.; Hartmann, H.; Besmehn, A.; Palkovits, R.;
18
19
20
21 Beller, M., Superior activity and selectivity of heterogenized cobalt catalysts for
22
23
24
25 hydrogenation of nitroarenes. *Catal. Sci. Technol.* **2019**, *9* (1), 157-162.
26
27
28 78. Ryabchuk, P.; Agapova, A.; Kreyenschulte, C.; Lund, H.; Junge, H.; Junge, K.;
29
30
31 Beller, M., Heterogeneous nickel-catalysed reversible, acceptorless
32
33
34
35 dehydrogenation of N-heterocycles for hydrogen storage. *Chem. Commun.* **2019**,
36
37
38
39 *55* (34), 4969-4972.
40
41
42 79. Lange, S.; Formenti, D.; Lund, H.; Kreyenschulte, C.; Agostini, G.; Bartling, S.;
43
44
45
46 Bachmann, S.; Scalone, M.; Junge, K.; Beller, M., Additive-Free Nickel-Catalyzed
47
48
49 Debenzylation Reactions via Hydrogenative C–O and C–N Bond Cleavage. *ACS*
50
51
52
53 *Sustainable Chem. Eng.* **2019**, *7* (20), 17107-17113.
54
55
56
57
58
59
60

- 1
2
3
4 80. Wu, Y.; Wang, T.; Wang, H.; Wang, X.; Dai, X.; Shi, F., Active catalyst construction
5
6
7 for CO₂ recycling via catalytic synthesis of N-doped carbon on supported Cu. *Nat.*
8
9
10 *Commun.* **2019**, *10* (1), 2599.
11
12
13
14 81. Xu, L.; Nie, R.; Lyu, X.; Wang, J.; Lu, X., Selective hydrogenation of furfural to
15
16
17 furfuryl alcohol without external hydrogen over N-doped carbon confined Co
18
19
20
21 catalysts. *Fuel Process. Technol.* **2020**, *197*, 106205.
22
23
24 82. Zhong, W.; Liu, H.; Bai, C.; Liao, S.; Li, Y., Base-Free Oxidation of Alcohols to
25
26
27 Esters at Room Temperature and Atmospheric Conditions using Nanoscale Co-
28
29
30
31 Based Catalysts. *Acs Catal.* **2015**, *5* (3), 1850-1856.
32
33
34
35 83. Zhou, Y.-X.; Chen, Y.-Z.; Cao, L.; Lu, J.; Jiang, H.-L., Conversion of a metal-
36
37
38 organic framework to N-doped porous carbon incorporating Co and CoO
39
40
41
42 nanoparticles: direct oxidation of alcohols to esters. *Chem. Commun.* **2015**, *51*
43
44
45 (39), 8292-8295.
46
47
48
49 84. Shen, K.; Chen, X.; Chen, J.; Li, Y., Development of MOF-Derived Carbon-Based
50
51
52 Nanomaterials for Efficient Catalysis. *Acs Catal.* **2016**, *6* (9), 5887-5903.
53
54
55
56
57
58
59
60

- 1
2
3
4 85. Bai, C.; Li, A.; Yao, X.; Liu, H.; Li, Y., Efficient and selective aerobic oxidation of
5
6
7 alcohols catalysed by MOF-derived Co catalysts. *Green Chem.* **2016**, *18*(4), 1061-
8
9
10 1069.
11
12
13
14 86. Jagadeesh, R. V.; Murugesan, K.; Alshammari, A. S.; Neumann, H.; Pohl, M.-M.;
15
16
17 Radnik, J.; Beller, M., MOF-derived cobalt nanoparticles catalyze a general
18
19
20 synthesis of amines. *Science* **2017**, *358*(6361), 326.
21
22
23
24 87. Dang, S.; Zhu, Q.-L.; Xu, Q., Nanomaterials derived from metal–organic
25
26
27 frameworks. *Nature Reviews Materials* **2017**, *3*(1), 17075.
28
29
30
31 88. Fang, R.; Tian, P.; Yang, X.; Luque, R.; Li, Y., Encapsulation of ultrafine metal-
32
33
34 oxide nanoparticles within mesopores for biomass-derived catalytic applications.
35
36
37
38 *Chem. Sci.* **2018**, *9*(7), 1854-1859.
39
40
41
42 89. Wang, Q.; Tsumori, N.; Kitta, M.; Xu, Q., Fast Dehydrogenation of Formic Acid
43
44
45 over Palladium Nanoparticles Immobilized in Nitrogen-Doped Hierarchically
46
47
48 Porous Carbon. *Acs Catal.* **2018**, *8*(12), 12041-12045.
49
50
51
52 90. Zhang, W.; Wu, W.; Long, Y.; Wang, F.; Ma, J., Co-Ag alloy protected by nitrogen
53
54
55 doped carbon as highly efficient and chemoselective catalysts for the
56
57
58
59
60

- hydrogenation of halogenated nitrobenzenes. *J. Colloid Interface Sci.* **2018**, *522*, 217-227.
91. Bennedsen, N. R.; Kramer, S.; Mielby, J. J.; Kegnæs, S., Cobalt–nickel alloy catalysts for hydrosilylation of ketones synthesized by utilizing metal–organic framework as template. *Catal. Sci. Technol.* **2018**, *8* (9), 2434-2440.
92. Bhadra, B. N.; Vinu, A.; Serre, C.; Jhung, S. H., MOF-derived carbonaceous materials enriched with nitrogen: Preparation and applications in adsorption and catalysis. *Mater. Today* **2019**, *25*, 88-111.
93. Lee, K. J.; Lee, J. H.; Jeoung, S.; Moon, H. R., Transformation of Metal–Organic Frameworks/Coordination Polymers into Functional Nanostructured Materials: Experimental Approaches Based on Mechanistic Insights. *Acc. Chem. Res.* **2017**, *50* (11), 2684-2692.
94. Nandi, S.; Saha, A.; Patel, P.; Khan, N.-u. H.; Kureshy, R. I.; Panda, A. B., Hydrogenation of Furfural with Nickel Nanoparticles Stabilized on Nitrogen-Rich Carbon Core–Shell and Its Transformations for the Synthesis of γ -Valerolactone in Aqueous Conditions. *ACS Appl. Mater. Interfaces* **2018**, *10* (29), 24480-24490.

- 1
2
3
4 95. Murugesan, K.; Senthamarai, T.; Alshammari, A. S.; Altamimi, R. M.;
5
6
7 Kreyenschulte, C.; Pohl, M.-M.; Lund, H.; Jagadeesh, R. V.; Beller, M., Cobalt-
8
9
10 Nanoparticles Catalyzed Efficient and Selective Hydrogenation of Aromatic
11
12
13 Hydrocarbons. *Acs Catal.* **2019**, *9* (9), 8581-8591.
14
15
16
17 96. Mondal, D.; Sharma, M.; Wang, C.-H.; Lin, Y.-C.; Huang, H.-C.; Saha, A.; Nataraj,
18
19
20 S. K.; Prasad, K., Deep eutectic solvent promoted one step sustainable conversion
21
22
23 of fresh seaweed biomass to functionalized graphene as a potential
24
25
26
27 electrocatalyst. *Green Chem.* **2016**, *18* (9), 2819-2826.
28
29
30
31 97. Yao, W.-T.; Yu, L.; Yao, P.-F.; Wei, K.; Han, S.-L.; Chen, P.; Xie, J.-S., Bulk
32
33
34 Production of Nonprecious Metal Catalysts from Cheap Starch as Precursor and
35
36
37 Their Excellent Electrochemical Activity. *ACS Sustainable Chem. Eng.* **2016**, *4* (6),
38
39
40
41 3235-3244.
42
43
44
45 98. Ji, G.; Duan, Y.; Zhang, S.; Fei, B.; Chen, X.; Yang, Y., Selective
46
47
48 Semihydrogenation of Alkynes Catalyzed by Pd Nanoparticles Immobilized on
49
50
51 Heteroatom-Doped Hierarchical Porous Carbon Derived from Bamboo Shoots.
52
53
54
55 *ChemSusChem* **2017**, *10* (17), 3427-3434.
56
57
58
59
60

- 1
2
3
4 99. Yang, H.; Nie, R.; Xia, W.; Yu, X.; Jin, D.; Lu, X.; Zhou, D.; Xia, Q., Co embedded
5
6
7 within biomass-derived mesoporous N-doped carbon as an acid-resistant and
8
9
10 chemoselective catalyst for transfer hydrodeoxygenation of biomass with formic
11
12
13 acid. *Green Chem.* **2017**, *19* (23), 5714-5722.
14
15
16
17 100. Duan, Y.; Ji, G.; Zhang, S.; Chen, X.; Yang, Y., Additive-modulated switchable
18
19
20 reaction pathway in the addition of alkynes with organosilanes catalyzed by
21
22
23 supported Pd nanoparticles: hydrosilylation versus semihydrogenation. *Catal. Sci.*
24
25
26
27 *Technol.* **2018**, *8* (4), 1039-1050.
28
29
30
31 101. Duan, Y.; Song, T.; Dong, X.; Yang, Y., Enhanced catalytic performance of cobalt
32
33
34 nanoparticles coated with a N,P-codoped carbon shell derived from biomass for
35
36
37 transfer hydrogenation of functionalized nitroarenes. *Green Chem.* **2018**, *20* (12),
38
39
40
41 2821-2828.
42
43
44
45 102. Song, T.; Ren, P.; Duan, Y.; Wang, Z.; Chen, X.; Yang, Y., Cobalt nanocomposites
46
47
48 on N-doped hierarchical porous carbon for highly selective formation of anilines
49
50
51 and imines from nitroarenes. *Green Chem.* **2018**, *20* (20), 4629-4637.
52
53
54
55
56
57
58
59
60

- 1
2
3
4 103. Ma, Z.; Song, T.; Yuan, Y.; Yang, Y., Synergistic catalysis on Fe–Nx sites and Fe
5
6
7 nanoparticles for efficient synthesis of quinolines and quinazolinones via oxidative
8
9
10 coupling of amines and aldehydes. *Chem. Sci.* **2019**, *10* (44), 10283-10289.
11
12
13
14 104. Zhou, S.; Dai, F.; Dang, C.; Wang, M.; Liu, D.; Lu, F.; Qi, H., Scale-up biopolymer-
15
16
17 chelated fabrication of cobalt nanoparticles encapsulated in N-enriched graphene
18
19
20 shells for biofuel upgrade with formic acid. *Green Chem.* **2019**, *21* (17), 4732-4747.
21
22
23
24 105. Zhang, W.; Oulego, P.; Slot, T. K.; Rothenberg, G.; Shiju, N. R., Selective Aerobic
25
26
27 Oxidation of Lactate to Pyruvate Catalyzed by Vanadium-Nitrogen-Doped Carbon
28
29
30 Nanosheets. *ChemCatChem* **2019**, *11* (15), 3381-3387.
31
32
33
34
35 106. Chen, X.; Yang, H.; Yan, N., Shell Biorefinery: Dream or Reality? *Chem. Eur. J.*
36
37
38 **2016**, *22* (38), 13402-13421.
39
40
41
42 107. Zhao, L.; Baccile, N.; Gross, S.; Zhang, Y.; Wei, W.; Sun, Y.; Antonietti, M.; Titirici,
43
44
45 M.-M., Sustainable nitrogen-doped carbonaceous materials from biomass
46
47
48 derivatives. *Carbon* **2010**, *48* (13), 3778-3787.
49
50
51
52 108. Primo, A.; Atienzar, P.; Sanchez, E.; Delgado, J. M.; García, H., From biomass
53
54
55 wastes to large-area, high-quality, N-doped graphene: catalyst-free carbonization
56
57
58
59
60

- of chitosan coatings on arbitrary substrates. *Chem. Commun.* **2012**, *48*(74), 9254-9256.
109. Dhakshinamoorthy, A.; Primo, A.; Concepcion, P.; Alvaro, M.; Garcia, H., Doped Graphene as a Metal-Free Carbocatalyst for the Selective Aerobic Oxidation of Benzylic Hydrocarbons, Cyclooctane and Styrene. *Chem. Eur. J.* **2013**, *19*(23), 7547-7554.
110. Primo, A.; Neatu, F.; Florea, M.; Parvulescu, V.; Garcia, H., Graphenes in the absence of metals as carbocatalysts for selective acetylene hydrogenation and alkene hydrogenation. *Nat. Commun.* **2014**, *5*(1), 5291.
111. Liu, Q.; Duan, Y.; Zhao, Q.; Pan, F.; Zhang, B.; Zhang, J., Direct Synthesis of Nitrogen-Doped Carbon Nanosheets with High Surface Area and Excellent Oxygen Reduction Performance. *Langmuir* **2014**, *30*(27), 8238-8245.
112. Lavorato, C.; Primo, A.; Molinari, R.; Garcia, H., N-Doped Graphene Derived from Biomass as a Visible-Light Photocatalyst for Hydrogen Generation from Water/Methanol Mixtures. *Chem. Eur. J.* **2014**, *20*(1), 187-194.

- 1
2
3
4 113. Hao, P.; Zhao, Z.; Leng, Y.; Tian, J.; Sang, Y.; Boughton, R. I.; Wong, C. P.; Liu,
5
6
7 H.; Yang, B., Graphene-based nitrogen self-doped hierarchical porous carbon
8
9
10 aerogels derived from chitosan for high performance supercapacitors. *Nano*
11
12
13 *Energy* **2015**, *15*, 9-23.
14
15
16
17 114. Wang, Y.-Y.; Hou, B.-H.; Lü, H.-Y.; Wan, F.; Wang, J.; Wu, X.-L., Porous N-doped
18
19
20 carbon material derived from prolific chitosan biomass as a high-performance
21
22
23 electrode for energy storage. *RSC Adv.* **2015**, *5*(118), 97427-97434.
24
25
26
27
28 115. Wu, T. X.; Wang, G. Z.; Zhang, X.; Chen, C.; Zhang, Y. X.; Zhao, H. J.,
29
30
31 Transforming chitosan into N-doped graphitic carbon electrocatalysts. *Chem.*
32
33
34 *Commun.* **2015**, *51* (7), 1334-1337.
35
36
37
38 116. Deng, J.; Li, M.; Wang, Y., Biomass-derived carbon: synthesis and applications in
39
40
41 energy storage and conversion. *Green Chem.* **2016**, *18* (18), 4824-4854.
42
43
44
45 117. Zhao, J.; Liu, Y.; Quan, X.; Chen, S.; Yu, H.; Zhao, H., Nitrogen-doped carbon with
46
47
48 a high degree of graphitization derived from biomass as high-performance
49
50
51 electrocatalyst for oxygen reduction reaction. *Appl. Surf. Sci.* **2017**, *396*, 986-993.
52
53
54
55
56
57
58
59
60

- 1
2
3
4 118. Raghavan, N.; Thangavel, S.; Venugopal, G., A short review on preparation of
5
6
7 graphene from waste and bioprecursors. *Applied Materials Today* **2017**, *7*, 246-
8
9
10 254.
11
12
13
14 119. Rizescu, C.; Podolean, I.; Albero, J.; Parvulescu, V. I.; Coman, S. M.; Bucur, C.;
15
16
17 Puche, M.; Garcia, H., N-Doped graphene as a metal-free catalyst for glucose
18
19
20 oxidation to succinic acid. *Green Chem.* **2017**, *19*(8), 1999-2005.
21
22
23
24 120. Garcia, A.; Albero, J.; García, H., Multilayer N-doped Graphene Films as
25
26
27 Photoelectrodes for H₂ Evolution. *ChemPhotoChem* **2017**, *1*(9), 388-392.
28
29
30
31 121. Esteve-Adell, I.; He, J.; Ramiro, F.; Atienzar, P.; Primo, A.; García, H., Catalyst-
32
33
34 free one step synthesis of large area vertically stacked N-doped graphene-boron
35
36
37 nitride heterostructures from biomass source. *Nanoscale* **2018**, *10*(9), 4391-4397.
38
39
40
41 122. He, J.; Anouar, A.; Primo, A.; García, H., Quality Improvement of Few-Layers
42
43
44 Defective Graphene from Biomass and Application for H₂ Generation.
45
46
47
48 *Nanomaterials* **2019**, *9*, 895.
49
50
51
52 123. Varma, A. J.; Deshpande, S. V.; Kennedy, J. F., Metal complexation by chitosan
53
54
55
56 and its derivatives: a review. *Carbohydr. Polym.* **2004**, *55*(1), 77-93.
57
58
59
60

- 1
2
3
4 124. Guibal, E., Interactions of metal ions with chitosan-based sorbents: a review. *Sep.*
5
6
7 *Purif. Technol.* **2004**, *38* (1), 43-74.
8
9
10
11 125. Wang, X.; Du, Y.; Fan, L.; Liu, H.; Hu, Y., Chitosan- metal complexes as
12
13 antimicrobial agent: Synthesis, characterization and Structure-activity study.
14
15
16
17 *Polym. Bull.* **2005**, *55* (1), 105-113.
18
19
20
21 126. Guibal, E., Heterogeneous catalysis on chitosan-based materials: a review. *Prog.*
22
23
24 *Polym. Sci.* **2005**, *30* (1), 71-109.
25
26
27
28 127. Taboada, E.; Cabrera, G.; Jimenez, R.; Cardenas, G., A kinetic study of the
29
30 thermal degradation of chitosan-metal complexes. *J. Appl. Polym. Sci.* **2009**, *114*
31
32
33
34
35 (4), 2043-2052.
36
37
38
39 128. Yan, N.; Chen, X., Sustainability: Don't waste seafood waste. *Nature* **2015**, *524*,
40
41
42 155-157.
43
44
45 129. Blandez, J. F.; Primo, A.; Asiri, A. M.; Álvaro, M.; García, H., Copper Nanoparticles
46
47 Supported on Doped Graphenes as Catalyst for the Dehydrogenative Coupling of
48
49
50
51 Silanes and Alcohols. *Angew. Chem. Int. Ed.* **2014**, *53* (46), 12581-12586.
52
53
54
55
56
57
58
59
60

- 1
2
3
4 130. Primo, A.; Esteve-Adell, I.; Blandez, J. F.; Dhakshinamoorthy, A.; Álvaro, M.;
5
6
7 Candu, N.; Coman, S. M.; Parvulescu, V. I.; García, H., High catalytic activity of
8
9
10 oriented 2.0.0 copper(I) oxide grown on graphene film. *Nat. Commun.* **2015**, *6*(1),
11
12
13
14 8561.
15
16
17
18 131. Hurtado, L.; Natividad, R.; García, H., Photocatalytic activity of Cu₂O supported on
19
20
21 multi layers graphene for CO₂ reduction by water under batch and continuous flow.
22
23
24 *Catal. Commun.* **2016**, *84*, 30-35.
25
26
27
28 132. Mateo, D.; Esteve-Adell, I.; Albero, J.; Primo, A.; García, H., Oriented 2.0.0 Cu₂O
29
30
31 nanoplatelets supported on few-layers graphene as efficient visible light
32
33
34 photocatalyst for overall water splitting. *Appl. Catal., B Environ.* **2017**, *201*, 582-
35
36
37
38 590.
39
40
41
42 133. Primo, A.; Esteve-Adell, I.; Coman, S. N.; Candu, N.; Parvulescu, V. I.; Garcia, H.,
43
44
45 One-Step Pyrolysis Preparation of 1.1.1 Oriented Gold Nanoplatelets Supported
46
47
48 on Graphene and Six Orders of Magnitude Enhancement of the Resulting Catalytic
49
50
51
52 Activity. *Angew. Chem. Int. Ed.* **2016**, *55*(2), 607-612.
53
54
55
56
57
58
59
60

- 1
2
3
4 134. Esteve-Adell, I.; Bakker, N.; Primo, A.; Hensen, E.; García, H., Oriented Pt
5
6
7 Nanoparticles Supported on Few-Layers Graphene as Highly Active Catalyst for
8
9
10 Aqueous-Phase Reforming of Ethylene Glycol. *ACS Appl. Mater. Interfaces* **2016**,
11
12
13
14 *8* (49), 33690-33696.
15
16
17
18 135. Dhakshinamoorthy, A.; Esteve Adell, I.; Primo, A.; Garcia, H., Enhanced Activity
19
20
21 of Ag Nanoplatelets on Few Layers of Graphene Film with Preferential Orientation
22
23
24 for Dehydrogenative Silane–Alcohol Coupling. *ACS Sustainable Chem. Eng.* **2017**,
25
26
27
28 *5* (3), 2400-2406.
29
30
31
32 136. Sahoo, B.; Surkus, A.-E.; Pohl, M.-M.; Radnik, J.; Schneider, M.; Bachmann, S.;
33
34
35 Scalone, M.; Junge, K.; Beller, M., A Biomass-Derived Non-Noble Cobalt Catalyst
36
37
38 for Selective Hydrodehalogenation of Alkyl and (Hetero)Aryl Halides. *Angew.*
39
40
41
42 *Chem. Int. Ed.* **2017**, *56* (37), 11242-11247.
43
44
45
46 137. Sahoo, B.; Formenti, D.; Topf, C.; Bachmann, S.; Scalone, M.; Junge, K.; Beller,
47
48
49 M., Biomass-Derived Catalysts for Selective Hydrogenation of Nitroarenes.
50
51
52
53 *ChemSusChem* **2017**, *10* (15), 3035-3039.
54
55
56
57
58
59
60

- 1
2
3
4 138. Scharnagl, F. K.; Hertrich, M. F.; Ferretti, F.; Kreyenschulte, C.; Lund, H.; Jackstell,
5
6
7 R.; Beller, M., Hydrogenation of terminal and internal olefins using a biowaste-
8
9
10 derived heterogeneous cobalt catalyst. *Science Advances* **2018**, *4* (9), eaau1248.
11
12
13
14 139. Hertrich, M. F.; Scharnagl, F. K.; Pews-Davtyan, A.; Kreyenschulte, C. R.; Lund,
15
16
17 H.; Bartling, S.; Jackstell, R.; Beller, M., Supported Cobalt Nanoparticles for
18
19
20 Hydroformylation Reactions. *Chem. Eur. J.* **2019**, *25* (21), 5534-5538.
21
22
23
24 140. Lee, D.-W.; Jin, M.-H.; Oh, D.; Lee, S.-W.; Park, J.-S., Straightforward Synthesis
25
26
27 of Hierarchically Porous Nitrogen-Doped Carbon via Pyrolysis of
28
29
30 Chitosan/Urea/KOH Mixtures and Its Application as a Support for Formic Acid
31
32
33
34 Dehydrogenation Catalysts. *ACS Sustainable Chem. Eng.* **2017**, *5* (11), 9935-
35
36
37
38 9944.
39
40
41
42 141. He, J.; Dhakshinamoorthy, A.; Primo, A.; Garcia, H., Iron Nanoparticles Embedded
43
44
45 in Graphitic Carbon Matrix as Heterogeneous Catalysts for the Oxidative C-N
46
47
48
49 Coupling of Aromatic N-H Compounds and Amides. *ChemCatChem* **2017**, *9* (15),
50
51
52 3003-3012.
53
54
55
56
57
58
59
60

- 1
2
3
4 142. Zhang, F.; Ma, C.; Chen, S.; Zhang, J.; Li, Z.; Zhang, X.-M., N-doped hierarchical
5
6
7 porous carbon anchored tiny Pd NPs: A mild and efficient quinolines selective
8
9
10 hydrogenation catalyst. *Mol. Catal.* **2018**, *452*, 145-153.
11
12
13
14 143. Bi, Q.-Y.; Lin, J.-D.; Liu, Y.-M.; He, H.-Y.; Huang, F.-Q.; Cao, Y., Dehydrogenation
15
16
17 of Formic Acid at Room Temperature: Boosting Palladium Nanoparticle Efficiency
18
19
20 by Coupling with Pyridinic-Nitrogen-Doped Carbon. *Angew. Chem. Int. Ed.* **2016**,
21
22
23
24 *55*(39), 11849-11853.
25
26
27
28 144. Chen, B.; Zhang, C.; Niu, L.; Shi, X.; Zhang, H.; Lan, X.; Bai, G., Biomass-Derived
29
30
31 N-doped Carbon Materials with Silica-Supported Ultrasmall ZnO Nanoparticles:
32
33
34 Robust Catalysts for the Green Synthesis of Benzimidazoles. *Chem. Eur. J.* **2018**,
35
36
37
38 *24*(14), 3481-3487.
39
40
41
42 145. Xu, M.; Zhao, J.; Shu, G.; Zheng, X.; Liu, Q.; Wang, Y.; Zeng, M., One-pot
43
44
45 carbonization of chitosan/P123/PdCl₂ blend hydrogel membranes to N-doped
46
47
48 carbon supported Pd catalytic composites for Ullmann reactions. *Int. J. Biol.*
49
50
51
52 *Macromol.* **2019**, *125*, 213-220.
53
54
55
56
57
58
59
60

- 1
2
3
4 146. Vasilev, A. A.; Efimov, M. N.; Bondarenko, G. N.; Muratov, D. G.; Dzidziguri, E. L.;
5
6
7 Ivantsov, M. I.; Kulikova, M. V.; Karpacheva, G. P., FeCo alloy nanoparticles
8
9
10 supported on IR pyrolyzed chitosan as catalyst for Fischer-Tropsch synthesis.
11
12
13
14 *Chem. Phys. Lett.* **2019**, *730*, 8-13.
15
16
17
18 147. Thombal, P. R.; Thombal, R. S.; Han, S. S., Chitosan-derived N-doped carbon
19
20
21 catalysts with a metallic core for the oxidative dehydrogenation of NH–NH bonds.
22
23
24 *RSC Adv.* **2020**, *10*(1), 474-481.
25
26
27
28 148. Liang, B.; Zhao, Y.; Li, K.; Lv, C., Porous carbon codoped with inherent nitrogen
29
30
31 and externally embedded cobalt nanoparticles as a high-performance cathode
32
33
34 catalyst for microbial fuel cells. *Appl. Surf. Sci.* **2020**, *505*, 144547.
35
36
37
38 149. Lin, Y.; Lu, G.-P.; Zhao, X.; Cao, X.; Yang, L.; Zhou, B.; Zhong, Q.; Chen, Z.,
39
40
41 Porous cobalt@N-doped carbon derived from chitosan for oxidative esterification
42
43
44 of 5-Hydroxymethylfurfural: The roles of zinc in the synthetic and catalytic process.
45
46
47
48 *Mol. Catal.* **2020**, *482*, 110695.
49
50
51
52
53
54
55
56
57
58
59
60

- 1
2
3
4 150. Zhang, L.; Wang, A.; Wang, W.; Huang, Y.; Liu, X.; Miao, S.; Liu, J.; Zhang, T.,
5
6
7 Co–N–C Catalyst for C–C Coupling Reactions: On the Catalytic Performance and
8
9
10 Active Sites. *Acs Catal.* **2015**, *5* (11), 6563-6572.
11
12
13
14 151. Liu, W.; Zhang, L.; Yan, W.; Liu, X.; Yang, X.; Miao, S.; Wang, W.; Wang, A.;
15
16
17 Zhang, T., Single-atom dispersed Co–N–C catalyst: structure identification and
18
19
20 performance for hydrogenative coupling of nitroarenes. *Chem. Sci.* **2016**, *7* (9),
21
22
23
24 5758-5764.
25
26
27
28 152. Tang, C.; Surkus, A.-E.; Chen, F.; Pohl, M.-M.; Agostini, G.; Schneider, M.; Junge,
29
30
31 H.; Beller, M., A Stable Nanocobalt Catalyst with Highly Dispersed Co_{Nx} Active
32
33
34 Sites for the Selective Dehydrogenation of Formic Acid. *Angew. Chem. Int. Ed.*
35
36
37
38 **2017**, *56* (52), 16616-16620.
39
40
41
42 153. Liu, W.; Zhang, L.; Liu, X.; Liu, X.; Yang, X.; Miao, S.; Wang, W.; Wang, A.; Zhang,
43
44
45 T., Discriminating Catalytically Active Fe_{Nx} Species of Atomically Dispersed Fe–
46
47
48 N–C Catalyst for Selective Oxidation of the C–H Bond. *J. Am. Chem. Soc.* **2017**,
49
50
51
52 *139* (31), 10790-10798.
53
54
55
56
57
58
59
60

- 1
2
3
4 154. Chen, Y.; Huang, Z.; Ma, Z.; Chen, J.; Tang, X., Fabrication, characterization, and
5
6
7 s tability of supported single-atom catalysts. *Catal. Sci. Technol.* **2017**, *7*(19), 4250-
8
9
10 4258.
11
12
13
14 155. Lai, W.-H.; Miao, Z.; Wang, Y.-X.; Wang, J.-Z.; Chou, S.-L., Atomic-Local
15
16
17 Environments of Single-Atom Catalysts: Synthesis, Electronic Structure, and
18
19
20
21 Activity. *Advanced Energy Materials* **2019**, *9*(43), 1900722.
22
23
24 156. Qiu, J.-Z.; Hu, J.; Lan, J.; Wang, L.-F.; Fu, G.; Xiao, R.; Ge, B.; Jiang, J., Pure
25
26
27 Siliceous Zeolite-Supported Ru Single-Atom Active Sites for Ammonia Synthesis.
28
29
30
31 *Chem. Mater.* **2019**, *31*(22), 9413-9421.
32
33
34
35 157. Gawande, M. B.; Fornasiero, P.; Zbořil, R., Carbon-Based Single-Atom Catalysts
36
37
38 for Advanced Applications. *Acs Catal.* **2020**, *10*(3), 2231-2259.
39
40
41
42 158. Li, Z.; Ji, S.; Liu, Y.; Cao, X.; Tian, S.; Chen, Y.; Niu, Z.; Li, Y., Well-Defined
43
44
45 Materials for Heterogeneous Catalysis: From Nanoparticles to Isolated Single-
46
47
48
49 Atom Sites. *Chem. Rev.* **2020**, *120*(2), 623-682.
50
51
52
53 159. Chen, W.; Pei, J.; He, C.-T.; Wan, J.; Ren, H.; Zhu, Y.; Wang, Y.; Dong, J.; Tian,
54
55
56 S.; Cheong, W.-C.; Lu, S.; Zheng, L.; Zheng, X.; Yan, W.; Zhuang, Z.; Chen, C.;
57
58
59
60

- Peng, Q.; Wang, D.; Li, Y., Rational Design of Single Molybdenum Atoms Anchored on N-Doped Carbon for Effective Hydrogen Evolution Reaction. *Angew. Chem. Int. Ed.* **2017**, *56* (50), 16086-16090.
160. Zhu, Y.; Sun, W.; Chen, W.; Cao, T.; Xiong, Y.; Luo, J.; Dong, J.; Zheng, L.; Zhang, J.; Wang, X.; Chen, C.; Peng, Q.; Wang, D.; Li, Y., Scale-Up Biomass Pathway to Cobalt Single-Site Catalysts Anchored on N-Doped Porous Carbon Nanobelt with Ultrahigh Surface Area. *Adv. Funct. Mater.* **2018**, *28* (37), 1802167.
161. Sommer, L. H.; Lyons, J. E., Stereochemistry of asymmetric silicon. XVI. Transition metal catalyzed substitution reactions of optically active organosilicon hydrides. *J. Am. Chem. Soc.* **1969**, *91* (25), 7061-7067.
162. Yamamoto, K.; Takemae, M., The Utility of t-Butyldimethylsilane as an Effective Silylation Reagent for the Protection of Functional Groups. *Bull. Chem. Soc. Jpn.* **1989**, *62* (6), 2111-2113.
163. Chung, M.-K.; Orlova, G.; Goddard, J. D.; Schlaf, M.; Harris, R.; Beveridge, T. J.; White, G.; Hallett, F. R., Regioselective Silylation of Sugars through Palladium

- Nanoparticle-Catalyzed Silane Alcoholysis. *J. Am. Chem. Soc.* **2002**, *124* (35), 10508-10518.
164. Raffa, P.; Evangelisti, C.; Vitulli, G.; Salvadori, P., First examples of gold nanoparticles catalyzed silane alcoholysis and silylative pinacol coupling of carbonyl compounds. *Tetrahedron Lett.* **2008**, *49* (20), 3221-3224.
165. Kim, S.; Kwon, M. S.; Park, J., Silylation of primary alcohols with recyclable ruthenium catalyst and hydrosilanes. *Tetrahedron Lett.* **2010**, *51* (34), 4573-4575.
166. Taguchi, T.; Isozaki, K.; Miki, K., Enhanced Catalytic Activity of Self-Assembled-Monolayer-Capped Gold Nanoparticles. *Adv. Mater.* **2012**, *24* (48), 6462-6467.
167. Mitschang, F.; Schmalz, H.; Agarwal, S.; Greiner, A., Tea-Bag-Like Polymer Nanoreactors Filled with Gold Nanoparticles. *Angew. Chem. Int. Ed.* **2014**, *53* (19), 4972-4975.
168. Li, Z.; Lin, S.; Ji, L.; Zhang, Z.; Zhang, X.; Ding, Y., Nanoporous palladium catalyzed silicon-based one-pot cross-coupling reaction of aryl iodides with organosilanes. *Catal. Sci. Technol.* **2014**, *4* (6), 1734-1737.

- 1
2
3
4 169. Li, Z.; Xu, X.; Zhang, X., Oxidation of Organosilanes with Nanoporous Copper as
5
6
7 a Sustainable Non-Noble-Metal Catalyst. *ChemPhysChem* **2015**, *16* (8), 1603-
8
9
10 1606.
11
12
13
14 170. Dhakshinamoorthy, A.; Concepcion, P.; Garcia, H., Dehydrogenative coupling of
15
16
17 silanes with alcohols catalyzed by $\text{Cu}_3(\text{BTC})_2$. *Chem. Commun.* **2016**, *52* (13),
18
19
20 2725-2728.
21
22
23
24 171. Wang, C.; Lin, X.; Ge, Y.; Shah, Z. H.; Lu, R.; Zhang, S., Silica-supported ultra
25
26
27 small gold nanoparticles as nanoreactors for the etherification of silanes. *RSC Adv.*
28
29
30 **2016**, *6* (104), 102102-102108.
31
32
33
34
35 172. Wang, C.; Zhang, Z.; Yang, G.; Chen, Q.; Yin, Y.; Jin, M., Creation of Controllable
36
37
38 High-Density Defects in Silver Nanowires for Enhanced Catalytic Property. *Nano*
39
40
41 *Lett.* **2016**, *16* (9), 5669-5674.
42
43
44
45 173. Schöbel, J.; Burgard, M.; Hils, C.; Dersch, R.; Dulle, M.; Volk, K.; Karg, M.; Greiner,
46
47
48 A.; Schmalz, H., Bottom-Up Meets Top-Down: Patchy Hybrid Nonwovens as an
49
50
51 Efficient Catalysis Platform. *Angew. Chem. Int. Ed.* **2017**, *56* (1), 405-408.
52
53
54
55
56
57
58
59
60

- 1
2
3
4 174. Lin, J.-D.; Bi, Q.-Y.; Tao, L.; Jiang, T.; Liu, Y.-M.; He, H.-Y.; Cao, Y.; Wang, Y.-D.,
5
6
7 Wettability-Driven Palladium Catalysis for Enhanced Dehydrogenative Coupling of
8
9
10 Organosilanes. *Acs Catal.* **2017**, *7*(3), 1720-1727.
11
12
13
14 175. Anbu, N.; Dhakshinamoorthy, A., Cu₃(BTC)₂ catalyzed dehydrogenative coupling
15
16
17 of dimethylphenylsilane with phenol and homocoupling of dimethylphenylsilane to
18
19
20 disiloxane. *J. Colloid Interface Sci.* **2017**, *490*, 430-435.
21
22
23
24 176. Dhiman, M.; Chalke, B.; Polshettiwar, V., Organosilane oxidation with a half million
25
26
27 turnover number using fibrous nanosilica supported ultrasmall nanoparticles and
28
29
30 pseudo-single atoms of gold. *J. Mater. Chem. A* **2017**, *5*(5), 1935-1940.
31
32
33
34
35 177. Dai, Y.; Xing, P.; Cui, X.; Li, Z.; Zhang, X., Coexistence of Cu(II) and Cu(I) in Cu
36
37
38 ion-doped zeolitic imidazolate frameworks (ZIF-8) for the dehydrogenative
39
40
41 coupling of silanes with alcohols. *Dalton Trans.* **2019**, *48*(44), 16562-16568.
42
43
44
45 178. Wang, C.; Li, X.; Jin, L.; Lu, P.-H.; Dejoie, C.; Zhu, W.; Wang, Z.; Bi, W.; Dunin-
46
47
48 Borkowski, R. E.; Chen, K.; Jin, M., Etching-Assisted Route to Heterophase Au
49
50
51 Nanowires with Multiple Types of Active Surface Sites for Silane Oxidation. *Nano*
52
53
54
55 *Lett.* **2019**, *19*(9), 6363-6369.
56
57
58
59
60

- 1
2
3
4 179. Li, H.; Guo, H.; Li, Z.; Wu, C.; Li, J.; Zhao, C.; Guo, S.; Ding, Y.; He, W.; Li, Y.,
5
6
7 Silylation reactions on nanoporous gold via homolytic Si–H activation of silanes.
8
9
10
11 *Chem. Sci.* **2018**, *9* (21), 4808-4813.
12
13
14 180. Wang, X.; Li, P.; Li, Z.; Chen, W.; Zhou, H.; Zhao, Y.; Wang, X.; Zheng, L.; Dong,
15
16
17 J.; Lin, Y.; Zheng, X.; Yan, W.; Yang, J.; Yang, Z.; Qu, Y.; Yuan, T.; Wu, Y.; Li, Y.,
18
19
20
21 2D MOF induced accessible and exclusive Co single sites for an efficient O-
22
23
24 silylation of alcohols with silanes. *Chem. Commun.* **2019**, *55* (46), 6563-6566.
25
26
27
28 181. Chen, B.; Li, F.; Mei, Q.; Yang, Y.; Liu, H.; Yuan, G.; Han, B., Synthesis of nitrogen
29
30
31 and sulfur co-doped hierarchical porous carbons and metal-free oxidative coupling
32
33
34 of silanes with alcohols. *Chem. Commun.* **2017**, *53* (97), 13019-13022.
35
36
37
38 182. Mitsudome, T.; Arita, S.; Mori, H.; Mizugaki, T.; Jitsukawa, K.; Kaneda, K.,
39
40
41 Supported Silver-Nanoparticle-Catalyzed Highly Efficient Aqueous Oxidation of
42
43
44 Phenylsilanes to Silanols. *Angew. Chem. Int. Ed.* **2008**, *47* (41), 7938-7940.
45
46
47
48 183. Kikukawa, Y.; Kuroda, Y.; Yamaguchi, K.; Mizuno, N., Diamond-Shaped [Ag₄]⁴⁺
49
50
51 Cluster Encapsulated by Silicotungstate Ligands: Synthesis and Catalysis of
52
53
54 Hydrolytic Oxidation of Silanes. *Angew. Chem. Int. Ed.* **2012**, *51* (10), 2434-2437.
55
56
57
58
59
60

- 1
2
3
4 184. Li, Z.; Zhang, C.; Tian, J.; Zhang, Z.; Zhang, X.; Ding, Y., Highly selective oxidation
5
6
7 of organosilanes with a reusable nanoporous silver catalyst. *Catal. Commun.*
8
9
10 **2014**, *53*, 53-56.
11
12
13
14 185. Teo, A. K. L.; Fan, W. Y., Catalytic hydrogen evolution from hydrolytic oxidation of
15
16
17 organosilanes with silver nitrate catalyst. *RSC Adv.* **2014**, *4* (71), 37645-37648.
18
19
20
21 186. Fan, L.; Liu, P. F.; Yan, X.; Gu, L.; Yang, Z. Z.; Yang, H. G.; Qiu, S.; Yao, X.,
22
23
24 Atomically isolated nickel species anchored on graphitized carbon for efficient
25
26
27 hydrogen evolution electrocatalysis. *Nat. Commun.* **2016**, *7* (1), 10667.
28
29
30
31 187. Zhang, H.; Wang, G.; Chen, D.; Lv, X.; Li, J., Tuning Photoelectrochemical
32
33
34 Performances of Ag-TiO₂ Nanocomposites via Reduction/Oxidation of Ag. *Chem.*
35
36
37 *Mater.* **2008**, *20* (20), 6543-6549.
38
39
40
41 188. Liu, Y.; Fang, L.; Lu, H.; Li, Y.; Hu, C.; Yu, H., One-pot pyridine-assisted synthesis
42
43
44 of visible-light-driven photocatalyst Ag/Ag₃PO₄. *Appl. Catal., B Environ.* **2012**,
45
46
47 *115-116*, 245-252.
48
49
50
51 189. Zhang, C.; Yu, K.; Feng, Y.; Chang, Y.; Yang, T.; Xuan, Y.; Lei, D.; Lou, L.-L.; Liu,
52
53
54
55 S., Novel 3DOM-SrTiO₃/Ag/Ag₃PO₄ ternary Z-scheme photocatalysts with
56
57
58
59
60

- 1
2
3
4 remarkably improved activity and durability for contaminant degradation. *Appl.*
5
6
7 *Catal., B Environ.* **2017**, *210*, 77-87.
8
9
- 10
11 190. Trench, A. B.; Machado, T. R.; Gouveia, A. F.; Assis, M.; da Trindade, L. G.;
12
13 Santos, C.; Perrin, A.; Perrin, C.; Oliva, M.; Andrés, J.; Longo, E., Connecting
14
15 structural, optical, and electronic properties and photocatalytic activity of
16
17 $\text{Ag}_3\text{PO}_4\text{:Mo}$ complemented by DFT calculations. *Appl. Catal., B Environ.* **2018**,
18
19 *238*, 198-211.
20
21
22
23
24
25
26
- 27
28 191. dos Santos, C. C.; de Assis, M.; Machado, T. R.; dos Santos Pereira, P. F.;
29
30 Minguez-Vega, G.; Cordoncillo, E.; Beltran-Mir, H.; Doñate-Buendía, C.; Andrés,
31
32 J.; Longo, E., Proof-of-Concept Studies Directed toward the Formation of Metallic
33
34 Ag Nanostructures from Ag_3PO_4 Induced by Electron Beam and Femtosecond
35
36 Laser. *Part. Part. Syst. Charact.* **2019**, *36* (6), 1800533.
37
38
39
40
41
42
43
44
- 45
46 192. Cerón Calloso, M.; Angulo-Cornejo, J. R.; Lino-Pacaheco, M. N.; Villanueva
47
48 Huerta, C. C.; Casimiro Soriano, E. M., Synthesis and characterization of silver(I)
49
50 complex with mixed ligands saccharinate and 2-(2-pyridyl)benzimidazole. *Rev.*
51
52 *Colomb. Quim.* **2018**, *47*, 73-78.
53
54
55
56
57
58
59
60

- 1
2
3
4 193. Aouadi, S. M.; Schultze, D. M.; Rohde, S. L.; Wong, K. C.; Mitchell, K. A. R.,
5
6
7 Growth and characterization of Cr₂N/CrN multilayer coatings. *Surf. Coat. Technol.*
8
9
10 2001, 140 (3), 269-277.
11
12
13
14 194. Yang, H.; Shang, L.; Zhang, Q.; Shi, R.; Waterhouse, G. I. N.; Gu, L.; Zhang, T., A
15
16
17 universal ligand mediated method for large scale synthesis of transition metal
18
19
20
21 single atom catalysts. *Nat. Commun.* 2019, 10 (1), 4585.
22
23
24 195. Bulushev, D. A.; Chuvilin, A. L.; Sobolev, V. I.; Stolyarova, S. G.; Shubin, Y. V.;
25
26
27 Asanov, I. P.; Ishchenko, A. V.; Magnani, G.; Riccò, M.; Okotrub, A. V.; Bulusheva,
28
29
30
31 L. G., Copper on carbon materials: stabilization by nitrogen doping. *J. Mater.*
32
33
34
35 *Chem. A* 2017, 5 (21), 10574-10583.
36
37
38 196. Lyutaya, M. D.; Kulik, O. P., Chemical properties of nitrides of some transition
39
40
41
42 metals. *Powder Metall. Met. Ceram.* 1970, 9 (10), 821-826.
43
44
45 197. Nam, N. D.; Kim, M. J.; Jo, D. S.; Kim, J. G.; Yoon, D. H., Corrosion protection of
46
47
48
49 Ti/TiN, Cr/TiN, Ti/CrN, and Cr/CrN multi-coatings in simulated proton exchange
50
51
52
53 membrane fuel cell environment. *Thin Solid Films* 2013, 545, 380-384.
54
55
56
57
58
59
60

- 1
2
3
4 198. Froment, F. F.; Bischoff, K. B., in *Chemical Reactor Analysis and Design*. 2nd ed.;
5
6
7 John Wiley: Berlin, 1990.
8
9
- 10 199. Butt, J. B., in *Reaction Kinetics and Reactor Design*. 2nd ed.; Marcel Dekker:
11
12
13 Berlin, 1999.
14
15
16
- 17 200. Serna, P.; Concepción, P.; Corma, A., Design of highly active and chemoselective
18
19
20 bimetallic gold–platinum hydrogenation catalysts through kinetic and isotopic
21
22
23 studies. *J. Catal.* **2009**, *265* (1), 19-25.
24
25
26
- 27 201. Milian, R.; Liu, L.; Boronat, M.; Corma, A., A new molecular pathway allows the
28
29
30 chemoselective reduction of nitroaromatics on non-noble metal catalysts. *J. Catal.*
31
32
33 **2018**, *364*, 19-30.
34
35
36
- 37 202. Bao, X.; Muhler, M.; Pettinger, B.; Schlögl, R.; Ertl, G., On the nature of the active
38
39
40 state of silver during catalytic oxidation of methanol. *Catal. Lett.* **1993**, *22* (3), 215-
41
42
43 225.
44
45
46
- 47 203. Waterhouse, G. I. N.; Bowmaker, G. A.; Metson, J. B., Oxygen chemisorption on
48
49
50 an electrolytic silver catalyst: a combined TPD and Raman spectroscopic study.
51
52
53
54
55
56 *Appl. Surf. Sci.* **2003**, *214* (1), 36-51.
57
58
59
60

- 1
2
3
4 204. Cao, E.; Firth, S.; McMillan, P. F.; Gavriilidis, A., Application of microfabricated
5
6
7 reactors for operando Raman studies of catalytic oxidation of methanol to
8
9
10 formaldehyde on silver. *Catal. Today* **2007**, *126* (1), 119-126.
11
12
13
14 205. Pulido, A.; Concepción, P.; Boronat, M.; Corma, A., Aerobic epoxidation of
15
16
17 propene over silver (111) and (100) facet catalysts. *J. Catal.* **2012**, *292*, 138-147.
18
19
20
21 206. Shimizu, K.-i.; Kubo, T.; Satsuma, A., Surface Oxygen-Assisted Pd Nanoparticle
22
23
24 Catalysis for Selective Oxidation of Silanes to Silanols. *Chem. Eur. J.* **2012**, *18* (8),
25
26
27 2226-2229.
28
29
30
31 207. Mori, K.; Tano, M.; Mizugaki, T.; Ebitani, K.; Kaneda, K., Efficient heterogeneous
32
33
34 oxidation of organosilanes to silanols catalysed by a hydroxyapatite-bound Ru
35
36
37 complex in the presence of water and molecular oxygen. *New J. Chem.* **2002**, *26*
38
39
40
41 (11), 1536-1538.
42
43
44
45 208. Mitsudome, T.; Yamamoto, Y.; Noudjima, A.; Mizugaki, T.; Jitsukawa, K.; Kaneda,
46
47
48 K., Highly Efficient Etherification of Silanes by Using a Gold Nanoparticle Catalyst:
49
50
51 Remarkable Effect of O₂. *Chem. Eur. J.* **2013**, *19* (43), 14398-14402.
52
53
54
55
56
57
58
59
60

- 1
2
3
4 209. Urayama, T.; Mitsudome, T.; Maeno, Z.; Mizugaki, T.; Jitsukawa, K.; Kaneda, K.,
5
6
7 O₂-enhanced Catalytic Activity of Gold Nanoparticles in Selective Oxidation of
8
9
10 Hydrosilanes to Silanols. *Chem. Lett.* **2015**, *44* (8), 1062-1064.
11
12
13
14 210. Voronova, E. D.; Golub, I. E.; Pavlov, A.; Belkova, N. V.; Filippov, O. A.; Epstein,
15
16
17 L. M.; Shubina, E. S., Dichotomous Si-H Bond Activation by Alkoxide and Alcohol
18
19
20 in Base-Catalyzed Dehydrocoupling of Silanes. *Inorg. Chem.* **2020**, *59* (17),
21
22
23
24 12240-12251.
25
26
27
28 211. Corriu, R. J. P.; Guerin, C.; Henner, B.; Wang, Q., Pentacoordinate
29
30
31 hydridosilicates: synthesis and some aspects of their reactivity. *Organometallics*
32
33
34
35 **1991**, *10* (7), 2297-2303.
36
37
38
39 212. Corriu, R.; Guérin, C.; Henner, B.; Wang, Q., Hydridosilicates: a new class of
40
41
42 pentacoordinated silicon derivatives with unusual properties. *Inorg. Chim. Acta*
43
44
45 **1992**, *198-200*, 705-713.
46
47
48
49 213. Chuit, C.; Corriu, R. J. P.; Reye, C.; Young, J. C., Reactivity of penta- and
50
51
52 hexacoordinate silicon compounds and their role as reaction intermediates. *Chem.*
53
54
55
56 *Rev.* **1993**, *93* (4), 1371-1448.
57
58
59
60

- 1
2
3
4 214. Lemos, P. S.; Silva, G. S.; Roca, R. A.; Assis, M.; Torres-Mendieta, R.; Beltrán-
5
6
7 Mir, H.; Mínguez-Vega, G.; Cordoncillo, E.; Andrés, J.; Longo, E., Laser and
8
9
10 electron beam-induced formation of Ag/Cr structures on Ag₂CrO₄. *PCCP* **2019**, *21*
11
12
13
14 (11), 6101-6111.
15
16
17 215. Assis, M.; Cordoncillo, E.; Torres-Mendieta, R.; Beltrán-Mir, H.; Mínguez-Vega, G.;
18
19
20 Oliveira, R.; Leite, E. R.; Foggi, C. C.; Vergani, C. E.; Longo, E.; Andrés, J.,
21
22
23
24 Towards the scale-up of the formation of nanoparticles on α-Ag₂WO₄ with
25
26
27 bactericidal properties by femtosecond laser irradiation. *Sci. Rep.* **2018**, *8* (1),
28
29
30
31 1884.
32
33
34 216. de Oliveira, R. C.; de Foggi, C. C.; Teixeira, M. M.; da Silva, M. D. P.; Assis, M.;
35
36
37
38 Francisco, E. M.; Pimentel, B. N. A. d. S.; Pereira, P. F. d. S.; Vergani, C. E.;
39
40
41
42 Machado, A. L.; Andres, J.; Gracia, L.; Longo, E., Mechanism of Antibacterial
43
44
45 Activity via Morphology Change of α-AgVO₃: Theoretical and Experimental
46
47
48
49 Insights. *ACS Appl. Mater. Interfaces* **2017**, *9*(13), 11472-11481.
50
51
52
53
54
55
56
57
58
59
60